REPORT DOCUMENTATION PAGE

1. AGENCY USE ONLY (Leave blank)	2. REPORT DATE	3. REPORT TYPE AND DATES COVERED
		FINAL TECHNICAL AUG 91-31 Jul 94

4. TITLE AND SUBTITLE

The Effect of Gravity on the Deposition of Thin Films: The Physical Vapor Transport of Copper Phthalocyanine

5. FUNDING NUMBERS

AFOSR-91-0297

61121OR

6. AUTHOR(S)

Prof. T.L. Einstein, Prof. M.E. Fisher
Prof. J.D. Weeks
Associated Investigator: Prof. J.A. Yorke

AFOSR-TR- 95-0226

7. PERFORMING ORGANIZATION NAME(S) AND ADDRESS(ES)

The University of Maryland
College Park, MD 20742

8. PERFORMING ORGANIZATION REPORT NUMBER

--

9. SPONSORING/MONITORING AGENCY NAME(S) AND ADDRESS(ES)

AFOSR
Building 410
Bolling AFB
Washington, D.C. 20332-6448

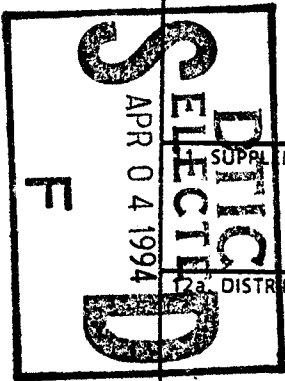**10. SPONSORING/MONITORING AGENCY REPORT NUMBER**

AFOSR-91-0297

11. SUPPLEMENTARY NOTES

--

12a. DISTRIBUTION/AVAILABILITY STATEMENT

Unlimited

Approved for public release;
distribution unlimited.

12b. DISTRIBUTION CODE

19950403 029

13. ABSTRACT (Maximum 200 words)

We describe our progress and final conclusions in our theoretical analysis of the growth of thin films of Copper Phthalocyanine (CuPc) via physical vapor transport using a closed cell ampoule. Three projects are discussed. The first is an analysis of the possibility of convection in the ampoule. This provides the most natural explanation for the experimental differences seen in thin films grown on earth and on the Space Shuttle. However we conclude that convection alone is unlikely to be able to explain these differences.

The other two projects examined general features of CuPc crystal growth arising from its very anisotropic shape. The second project modeled the CuPc molecule as a hard square shaped object and examined detailed features of the packing of such objects by a physically motivated deposition algorithm. The third project developed a more realistic intermolecular potential for CuPc involving attractive as well as repulsive intermolecular forces. Crystal structures and diffusion barriers were examined. These considerations have more general applicability to the crystal growth of anisotropic molecules on earth, and we believe further work along these lines is called for.

14. SUBJECT TERMS

Crystal Growth; Gravity; Convection

15. NUMBER OF PAGES

16. PRICE CODE

--

17. SECURITY CLASSIFICATION OF REPORT	18. SECURITY CLASSIFICATION OF THIS PAGE	19. SECURITY CLASSIFICATION OF ABSTRACT	20. LIMITATION OF ABSTRACT
Unclassified	Unclassified	Unclassified	Unlimited

DISCLAIMER NOTICE

UNCLASSIFIED

Technical Report
distributed by

DEFENSE
TECHNICAL
INFORMATION
CENTER

DTIC Acquiring Information-
Imparting Knowledge

Cameron Station
Alexandria, Virginia 22304-6145

UNCLASSIFIED

THIS DOCUMENT IS BEST QUALITY AVAILABLE. THE COPY FURNISHED TO DTIC CONTAINED A SIGNIFICANT NUMBER OF PAGES WHICH DO NOT REPRODUCE LEGIBLY.

Final Technical Report

A. *Objectives of the research effort*

As discussed in earlier Reports, our research effort was motivated by a set of experiments by Mark Debe and coworkers, which explored various features of the growth of crystalline thin films of Copper Phthalocyanine (CuPc) via physical vapor transport (PVT) using a closed-cell ampoule [1.1-1.4]. Films grown under a variety of conditions in microgravity on the Space Shuttle in low Earth orbit (LEO) were compared to ground control experiments at unit gravity. The major finding is that the center region of two films of CuPc produced in LEO are strikingly different from the edges and from both the centers and the edge region of the 13 ground-grown control films of equivalent thickness. In particular, the crystalline density is at least a factor of two greater at the center than at the edges or for the ground grown controls. The LEO central regions consisted of well-oriented, densely packed columnar structures--a morphology with desirable optical properties--while the unit gravity samples included only widely spaced narrow whiskers that appeared to be tangled and not well-oriented. In addition there is some evidence that the underlying crystalline polymorph may also vary between the two sets of samples.

The objective of the present research project was to understand the nature of the morphological selection in the PVT crystal growth process. One major goal has been to assess from a theoretical perspective what role gravity could play in producing the different morphologies seen in LEO. A second major goal has been to determine how the very anisotropic (platelike) shape of the CuPc molecule influences the crystal growth morphologies both on earth and in space. As indicated in detail below we have made good progress towards both these goals, though more work needs to be done. Because of the third year of our contract was not funded, we were not able to pursue some promising leads, and must leave some work to the future.

The most obvious way gravity could play a role is through its effect on convection in the cell. Accordingly, we devoted considerable effort to determining whether the geometry of the PVT cell, thermal gradients, and the density of enclosed gases are sufficient to induce convection at unit gravity. We have concluded that it is unlikely that significant convection can arise as a result of the one-dimensional (vertical) temperature gradient in Debe's experimental cell. A summary of our conclusions is given in Section B.1, and a detailed discussion is attached as Appendix A of this Report.

A major problem we faced in trying to assess the role of gravity was that very little is known about many aspects of thin film growth of large organic molecules even on earth. Therefore we also carried out research on how the morphology selection might be affected by the microscopic dynamics of surface diffusion and attachment of molecules on the crystal-vapor interface in general. We have made good progress in this research, and believe the ideas we introduced there will play an important role in any future research in this area.

The most striking feature of the CuPc molecule is its very anisotropic shape: it is essentially a flat square plate. See Fig. 1 Many features of the dynamics and crystal structure must be strongly influenced by this unusual shape. These shape considerations should have more general implications for the growth of organic thin films under a variety of conditions. Similar ideas have proved very useful in other contexts. Thus, the structure of liquid metals is well represented by a fluid of hard spheres of appropriate diameter, and basic features of the isotropic-to-nematic phase transition in liquid crystals is controlled by the anisotropic shape of the individual molecules[1.5].

As a first attempt to incorporate shape considerations into the growth of CuPc films, we have studied a simplified "hard square" model. Growth is modeled by the sequential attachment of planar square molecules whose only interactions are excluded volume interactions forbidding neighboring molecules to overlap. The most recent results from this

simulation project are summarized in Section B.2.

Lastly, we have focused much effort on constructing computationally feasible simulation models of CuPc crystal growth at the molecular scale, taking account of attractive as well as repulsive interactions. To reach this goal we have developed a simplified intermolecular potential and determined some of its low energy crystal structures. We have shown that the simplified models are capable of qualitatively reproducing some basic features of known CuPc crystal structures. We have also begun an investigation of the energetic and kinetics of diffusion of a single molecule near a fixed crystalline substrate. These results are summarized in Section B.3. A detailed Report is attached as Appendix B.

B. Status of the research effort

1. Studying the possibility of convection in Physical Vapor Transport (PVT) in ground-based and low Earth orbit (LEO) experiments (Fisher)

As indicated in our last Report, we have concluded that it is unlikely that significant convection can arise as a result of the one-dimensional (vertical) temperature gradient in Debe's experimental cell. This appears to rule out the most obvious explanation for the different behavior in LEO and the ground samples, and we have not pursued this line of research much since our last Report. We asked Professor Alexander Chernov, a world-renowned authority on both theoretical and experimental aspects of crystal growth, to review our conclusions. He agreed with our assessment, but mentioned that radial (horizontal) temperature gradients between the center and sidewalls of the cell are also present and could conceivably induce convection. However, a rough order of magnitude estimate suggests only a very small effect. A final Report detailing these conclusions is attached as Appendix A.

2. Microscopic models of stochastic growth with contact interactions (Einstein)

Research continued on simulated crystal growth using the square deposition computer program originally written by L. Kieffer Warman, and described in detail in a previous Report. The code produces an output file consisting of the positions of the centers of each square plus its orientation. A new square is accepted if its normal makes an angle with the square it first touches that is less than some specified critical angle, with an adjustable number (and distance) of lateral moves allowed if a trial exceeds this angle. Histograms of the orientation θ of the normal vector of each square, relative to the vertical direction, in a given pile were similar but not identical to gaussians, as illustrated in Fig. 2. This distribution was obtained by choosing θ randomly between 0 and π. To produce a spherically symmetric distribution of normals, one must choose a θ distribution that goes as $\sin \theta$. Histograms were made of the piles produced with this modified distribution, with quite different results: Instead of being peaked at 0 degrees, the histograms tended to be peaked at a value between 70° and 80°. The spherically symmetric distribution of square normals is seen to be a poor choice for modeling the growth of CuPc microcrystals, which have a herringbone structure with overlapping molecules having identical orientations. The spherical distribution of square normals, on the other hand, biases against such behavior, because only a relatively small number of horizontal squares are produced; the majority will be closer to the vertical. To model the configurations of CuPc more accurately, we turned to a distribution that favored squares with horizontal ($\theta = 0$) orientations, illustrated in Fig. 3.

Improvements were also made to the deposition algorithm. The version developed by Warman and used during the earliest work relied on a discrete approximation to check whether an incoming square made contact with previously deposited squares. Occasionally the code suggested that contact had been made when graphical displays showed that it had

not. As the grid was made finer, the height of a pile decreased, but it was difficult to assess the limiting situation due to limited memory and disk space. Hence, the program was revised (with considerable labor) to include an analytic determination of the point of contact between squares.

From the numerical data implicit in the piles, a major goal was to characterize and interpret the correlations of the orientation of squares as a function of their separation, in particular to find the form and characteristic length of the decay in orientation correlation of pairs of squares as their horizontal separation increased with vertical separation fixed, or *vice versa.* Initial work did show evidence of decay of orientational correlations with separation in either direction and strong net orientational alignment for the entire pile. In the first stage, we generated scatter plots to illustrate this tendency. Last summer we extended this approach to look at various statistical properties. The density was checked as a function of height z in the pile, as illustrated in Fig. 4. There is a very high density near the substrate, where the squares are nearly horizontal. The density decays quickly to a constant value perhaps half the near-substrate value (but dependent on the acceptance angle) and remains around this value until quite near the top of the pile, when it drops quickly to zero. We examined the correlations of tilt angle by computing $\langle(\theta(r)-\theta(0))^2\rangle$, where r is the horizontal distance from a reference square (averaged over the entire pile). Plotted vs. r, as in Fig. 5, this function quickly rises, then slowly decays. The height of the pile increased linearly with time, suggesting a steady-state growth process. We spent considerable effort in examining the roughness w of the piles, where w is the root-mean-square fluctuations of the height of the pile, averaged over r. A log-log plot of w vs. the average height at first grew linearly, then rather abruptly leveled out at a height that increased with the lateral dimension L of the pile, as shown in Fig. 6. As illustrated in Fig. 7, we also found that the L-dependence of w could be adequately described by the a two-parameter fit to the form $w^2 = c_1 + c_2*\ln(L)$, the behavior for the Edwards-Wilkinson model[2.1], which is expected at relatively early times. (Later on, the growth paradigm is expected to shift to Kardar-Parisi-Zhang[2.2] for this growth algorithm.) We did note that inconclusive evidence that for large L the roughness seemed to grow faster than the above equation.

Due to the premature termination of funding, we were not able to analyze these properties more systematically, nor to consider other properties of concern. E.g., we could not study how the density and volume of the piles depend on the amount of diffusion (hopping after unsuccessful adsorption attempts). We will also did not have time to develop simple models to compare with the simulated data. We reemphasize that the general problem of deposition of highly asymmetric objects has received almost no attention, in stark contrast to the many studies of deposition of spheres[2.3], and so seems a particularly fertile area for future study.

3. *Realistic intermolecular potential, crystal structures, and dynamics of growth (Weeks)*

As discussed in our previous reports, an empirical potential for the CuPc molecule is available from the standard CHARMM molecular modeling package, involving interatomic potentials for all the 57 atoms in the CuPc molecule [3.1]. Atom-atom model potentials of this kind have proved capable of fitting many properties of large organic and inorganic molecules, and programs such as CHARMM are routinely used to assess the feasibility of new compounds in drug design. The CHARMM potential for CuPc has been shown to fit one particular crystal structure of the material to very good accuracy. However, this potential requires a total of 57 x 57 = 3249 separate interaction terms to represent the total energy of just one pair of CuPc molecules, making large-scale simulations impossible due to the computational load.

The first question we addressed was whether it was possible to develop a simplified intermolecular potential which preserves essential features of the full potential while requiring much less computation. The idea was to represent groups of atoms in the original

molecule by *interaction sites*. We then tried to choose empirical potentials between interaction sites in different molecules to reproduce as closely as possible basic features of the full CuPc intermolecular potential as given by the CHARMM model. Particular attention was paid to the low energy "sliding" configurations where the planar molecules are parallel and the centers move relative to one another. These configurations should be very important for surface diffusion.

Clearly there is a tradeoff between an accurate representation of the full potential surfaces and a simple representation using only a few interaction sites. We do not know how to quantify this tradeoff and can only use our best judgment as to when an acceptable compromise has been achieved. In our final version, we introduced a model with 13 interaction sites, not all of which interact with each other. With this potential, the total number of terms needed to calculate the interaction of two molecules is brought down to 89. The computer time in typical applications was reduced by nearly a factor of 100. Memory requirements are also reduced by more than 3/4. A picture of the "model" molecule, superimposed over the CuPc molecule, is shown in Fig. 8.

Minimum energy crystal structures for this model potential were calculated using a multi-dimensional minimization code [3.2]. Multiple minimizations from different starting configurations yielded several different crystal structures that all had energies per unit cell within a few percent of the value for the full potential. CuPc is known to have several crystalline polymorphs. Unfortunately there is almost no information in the literature about the details of these different crystal structures. Thus we were not able to determine whether there is detailed correspondence between them and the minimum-energy structures we have found using our model potential. The main point, on which both our models and the experiments agree, is that CuPc has a number of different locally stable, low energy crystal structures, including those with a herringbone structure.

We could easily tune the parameters of our model further to reproduce even more features of any particular experimental crystal structure. However, our intention is not to accurately reproduce one particular crystal structure but to get an overall qualitatively accurate potential describing interactions of very anisotropic plate-like molecules in the *variety* of configurations encountered during the course of surface diffusion and crystal growth. For this purpose we believe our present potential should prove adequate. This work has been submitted for publication, and is presently under review at the Journal of Crystal Growth. A preprint of this work is attached as Appendix C.

Work has begun on a second project, and we hope to continue this further on our own and eventually produce a second publication. The idea is to determine the energy barriers and kinetics associated with diffusion of a single CuPc molecule on the cleaved surface of the CuPc crystal. Various techniques have been described in the literature [3.3] for mapping out the energy landscape for diffusion on a crystal surface. In our case we do not expect much relaxation of the crystal surface to occur during diffusion; thus we chose to use a simplified technique in which surface relaxation is neglected. However the extra degrees of freedom due to the non-spherical shape of the CuPc molecule still make this a challenging calculation.

We then plan to use transition-state theory [3.3] to estimate the kinetics of diffusion on this surface. We believe that surface diffusion may proceed in a very different way for such large anisotropic molecules than the usual hopping mode adopted by atoms, since *rotational* degrees of freedom must now play a significant role. Debe has rightly emphasized the crucial role surface diffusion must play in CuPc crystal growth, and further research along these lines is definitely called for.

C. Publications

A paper describing the construction of our simplified model potential for the CuPc molecule and the crystal structures it predicts has been submitted to the Journal of Crystal Growth and is presently under review. With some further work, we hope to write a second paper on surface diffusion with anisotropic molecules. We intend to write a short paper reporting the summer work on hard-square deposition, but are dependent on participation by the student. The Final Report in Appendix A describing our conclusions with regard to convection in the cell has been written in a very detailed form, to document thoroughly what we have done and to aid any future workers on this project. We plan to publish a short note giving our main conclusions, probably in the Journal of Crystal Growth.

D. Personnel associated with the research effort

- Senior Personnel: Professors T. L. Einstein, M. E. Fisher, and J. D. Weeks.

- Postdoctoral Associate: Dr. Robin Selinger

- Graduate students: Sheng-nan Lai and Dajiang Liu

- Summer Student: David R. Eisner

- Consultant: Professor Alex Chernov

E. Interactions

- Dr. Robin Selinger presented a paper at the March 1993 meeting of the American Physical Society entitled "Simulation studies of morphology selection in the growth of crystalline organic thin films." She also presented a seminar on this work at Georgetown University in March, 1994.

- Professor Alex Chernov read our preliminary technical report about the possibility of convection in the experimental cell. He visited the University of Maryland to consult with us about its conclusions and to offer his suggestions for future work.

References

[1.1] M. K. Debe, R. J. Poirier, E. L. Cook, L. R. Miller, M. S. Spiering, and S. P. Floeder, J. Vac. Sci. Technol. A **8** (1), p. 49 (1990).

[1.2] M. K. Debe, R. J. Poirier, D. D. Erickson, T. N. Tommet, D. R. Field and K. M. White, Thin Solid Films 186, p. 257 (1990).

[1.3] M. K. Debe and K. K. Kam, Thin Solid Films **186**, p.289 (1990).

[1.4] M. K. Debe and R. J. Poirier, Thin Solid Films **186**, p. 327 (1990).

[1.5] See, e.g., D. Chandler, J. D. Weeks and H. C. Andersen, Science **220**, p. 787 (1983).

[2.1] S. F. Edwards and D. R. Wilkinson, Proc. Roy. Soc. (London) **A381**, 17 (1982).

[2.2] M. Kardar, G. Parisi, and Y.-C. Zhang, Phys. Rev. Lett. **56**, 889 (1986).

[2.3] F. Family and T. Vicsek (eds.), *Dynamics of Fractal Surfaces* (World Scientific, Singapore, 1991) contains 45 important papers on this topic, including [2.1] and [2.2].

[3.1] Potential is given by the CHARMM software package; see B. R. Brooks *et al.*, J. Comp. Chem. **4**, 187 (1983). Values of the appropriate CHARMM interatomic potential parameters for CuPc were fit by Prof. Andrew Pohorille, private communication.

[3.2] Subroutine POWELL, from W. Press et al, in "Numerical Recipes" (Cambridge U. Press, 1992), p. 406.

[3.3] D. Srivastava and B. J. Garrison, J. Chem. Phys. **95**, 6885 (1991); Phys. Rev. B **46**, 1472 (1992).

Figure Captions

Fig. 1. Chemical constituents of CuPc. The molecule has a nearly square, planar structure with a side length of about 10 Å and a thickness of about 3.5 Å.

Fig. 2: Histogram of the orientation q (relative to the vertical direction) of 300,000 squares in a pile, obtained choosing the three Euler angles with a flat random distribution. The distributions were peaked at $\theta=0$ and decayed to zero in a qualitatively (but not quantitatively) gaussian manner. In addition, until θ reached the critical angle (here 15°), the curve was rather linear, as noted in earlier work. At the critical angle, a discontinuity in the slope is evident.

Fig. 3: Histogram of 300,000 squares in a pile, obtained from the more appropriate distribution function , where θ is measured in radians. (This distribution has a maximum at $\theta = 0$ and a minimum at $\theta = \pi/2$ radians.) As in the histogram in Fig. 1 produced using the original flat distribution of q values, the histograms of the square piles produced with the new distribution function were peaked at $\theta = 0$ and fell off towards zero as θ approached $\pi/2$ radians. Once again, discontinuity in slope is observed at the critical angle, here 15° as in Fig. 2.

Fig. 4: Density vs. z (coordinate in the growth direction) for a 1000x1000 deposition area.

Fig. 5: Orientational correlations vs. horizontal separation, averaged over the entire pile.

Fig. 6: Log-log plot of roughness (w) vs. mean height of the pile, for several values of the length of a side of the [square] deposition area, showing the sharp crossover to saturated roughness with increasing height.

Fig. 7: Plot of saturated mean square roughness (w^2) vs. the length of a side of the [square] deposition area, along with a best-fit to the Edwards-Wilkinson scaling form.

Fig. 8: The simplified molecular structure used in our model potential for CuPc. This should be compared to Fig. 1.
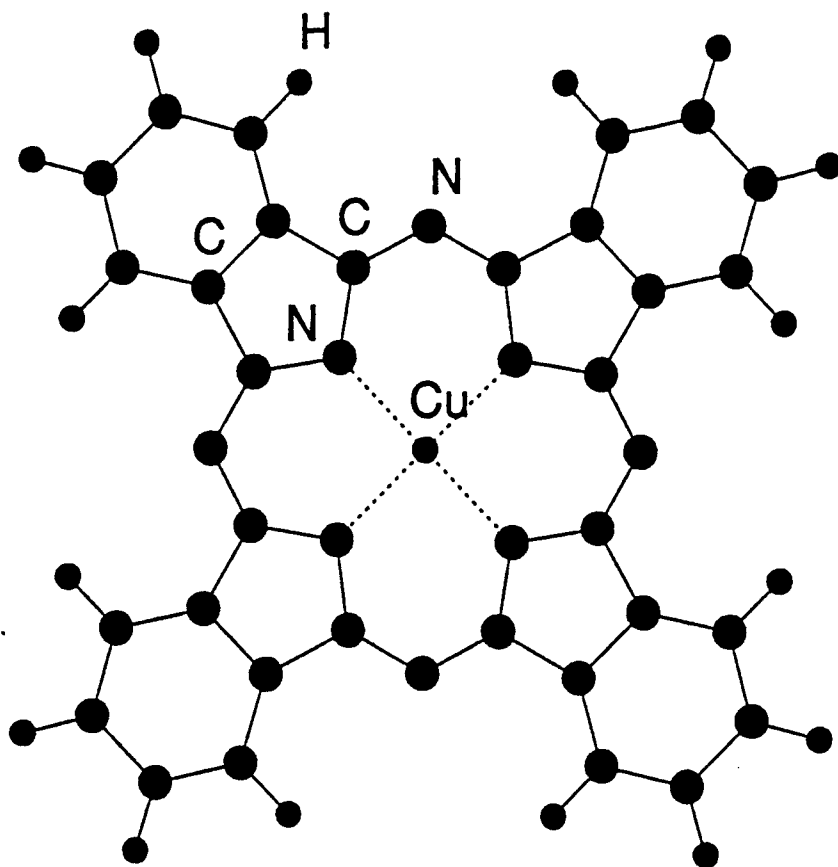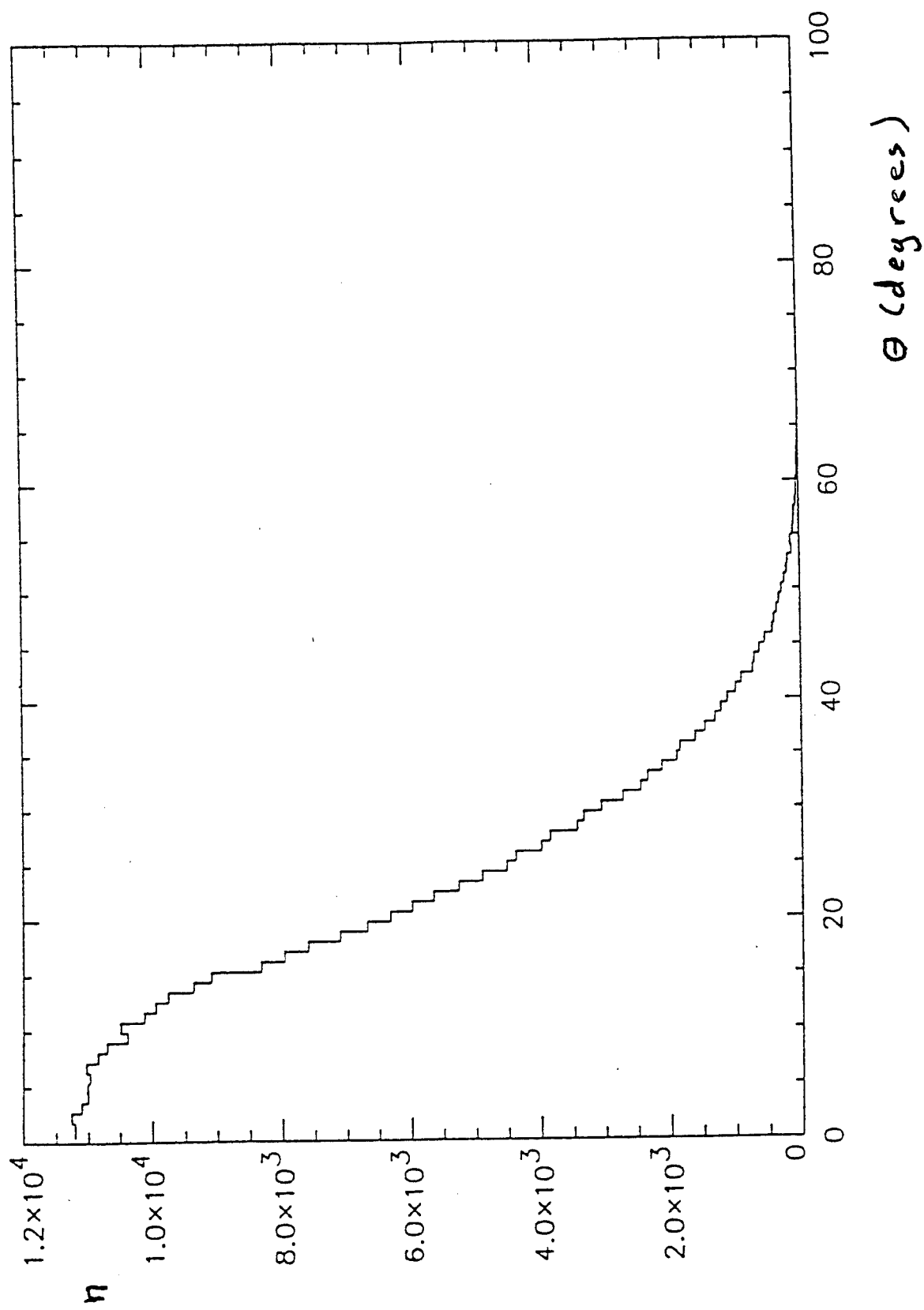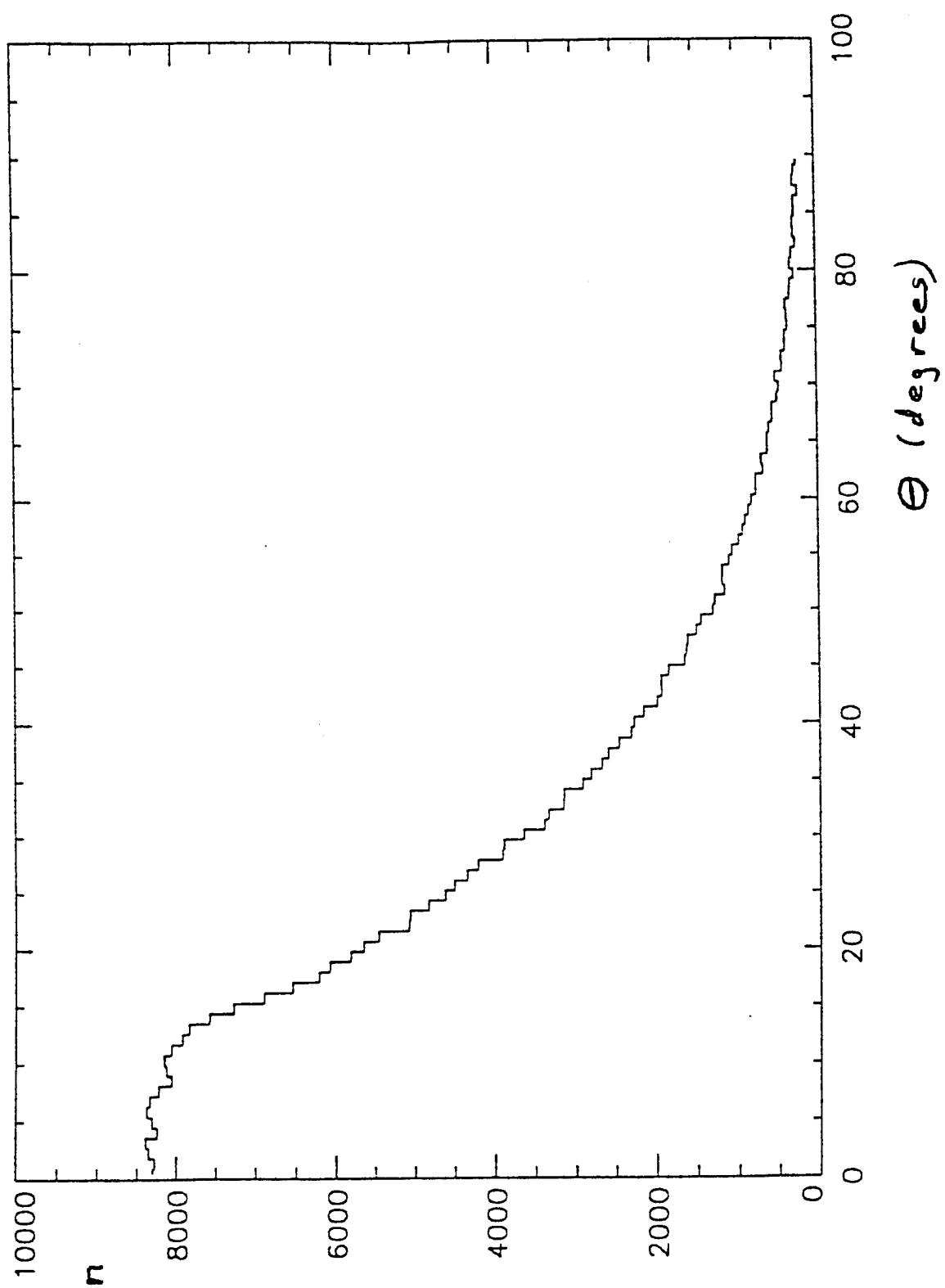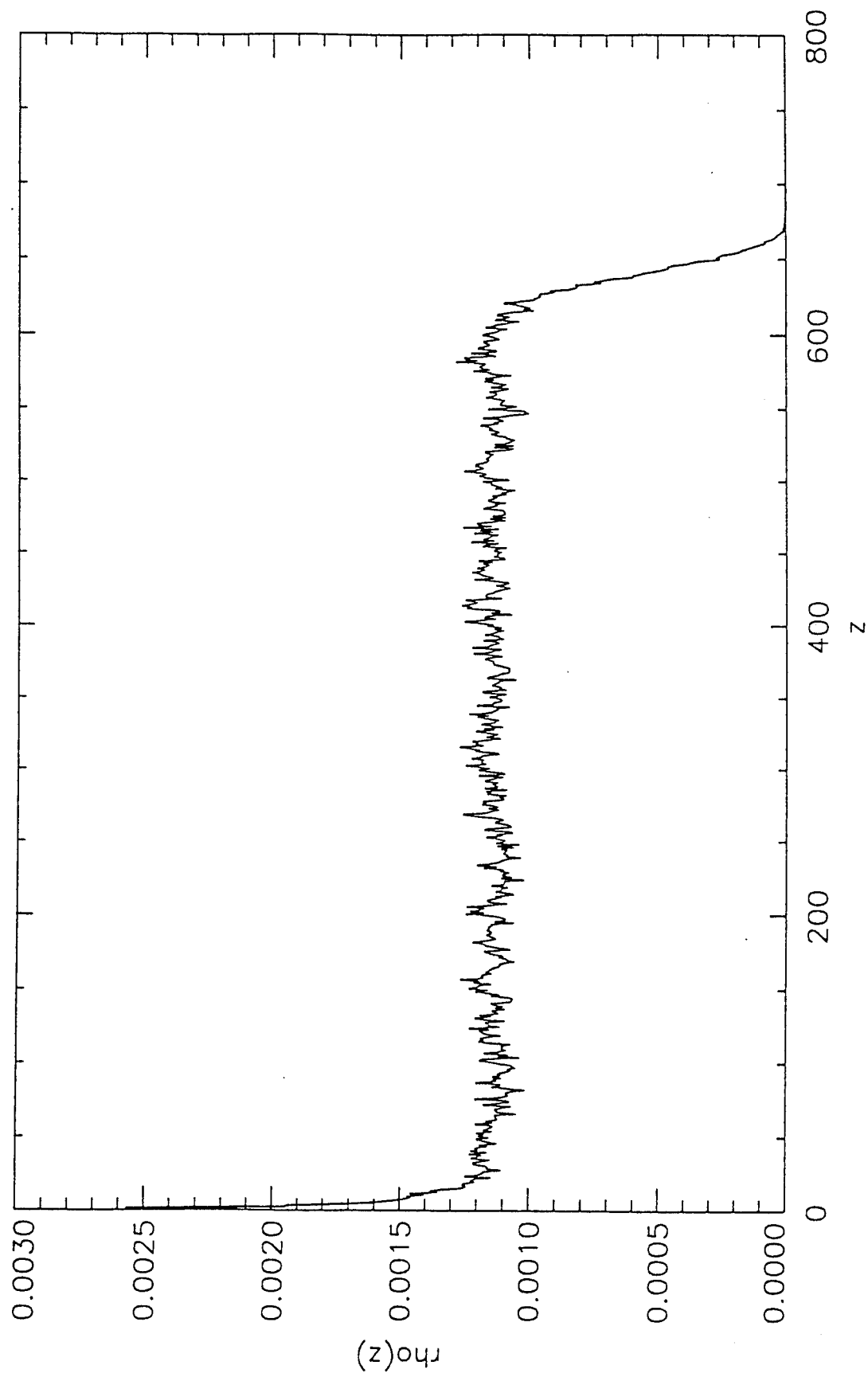
Fig. 1
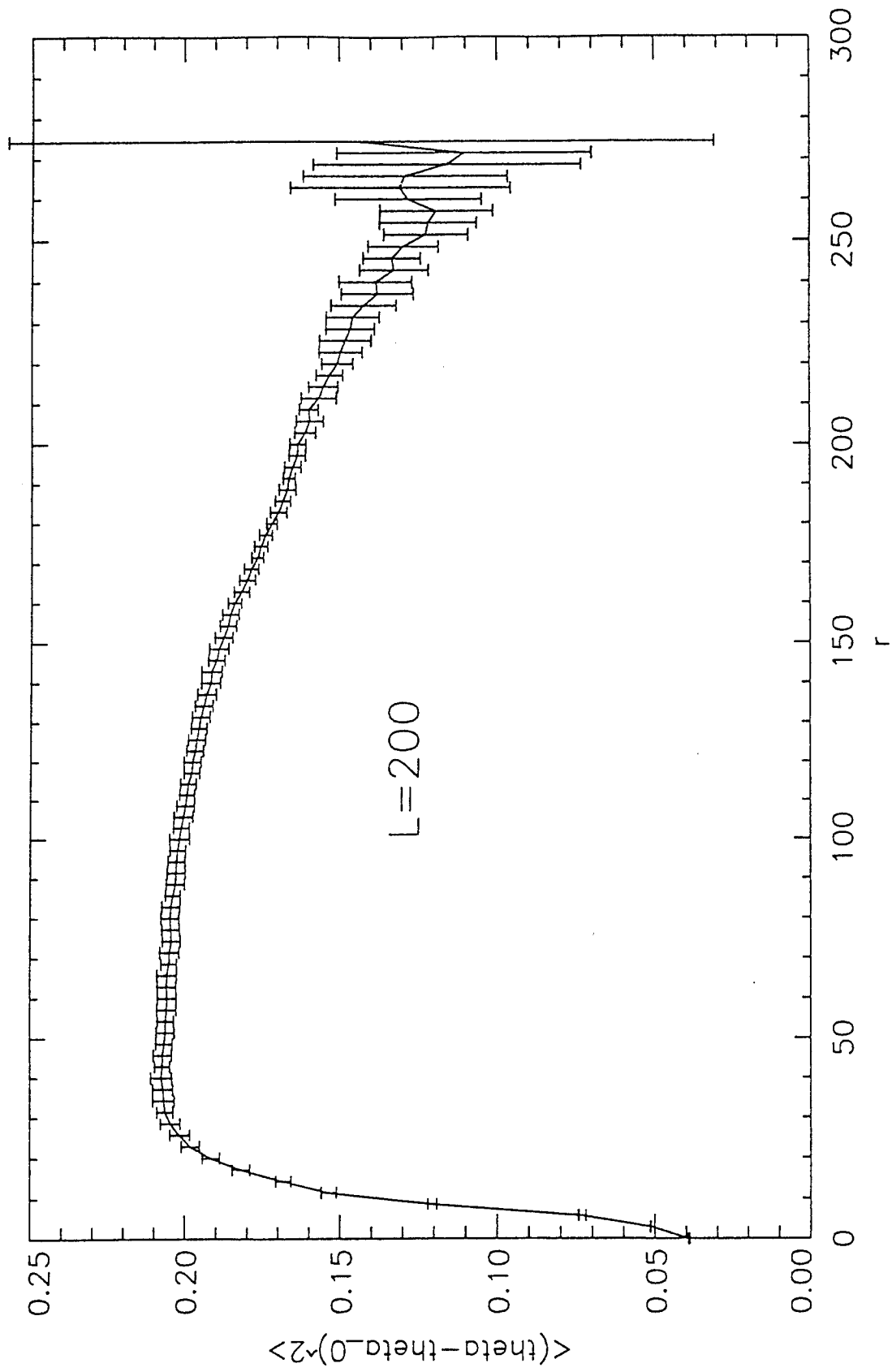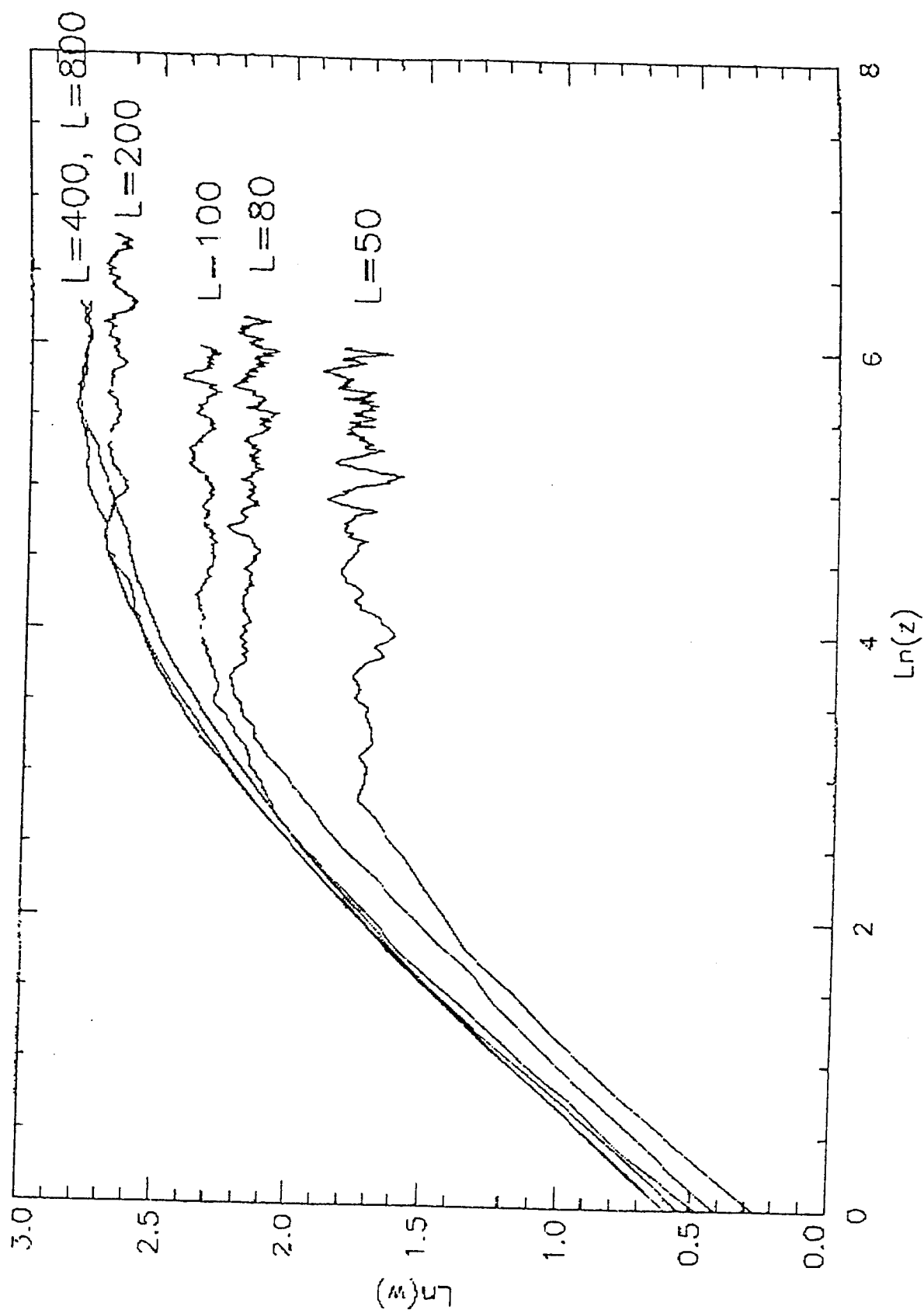
Fig 2

Fig 3

Fig 4

Fig 5

Fig 5

Fig 6

Fig 6
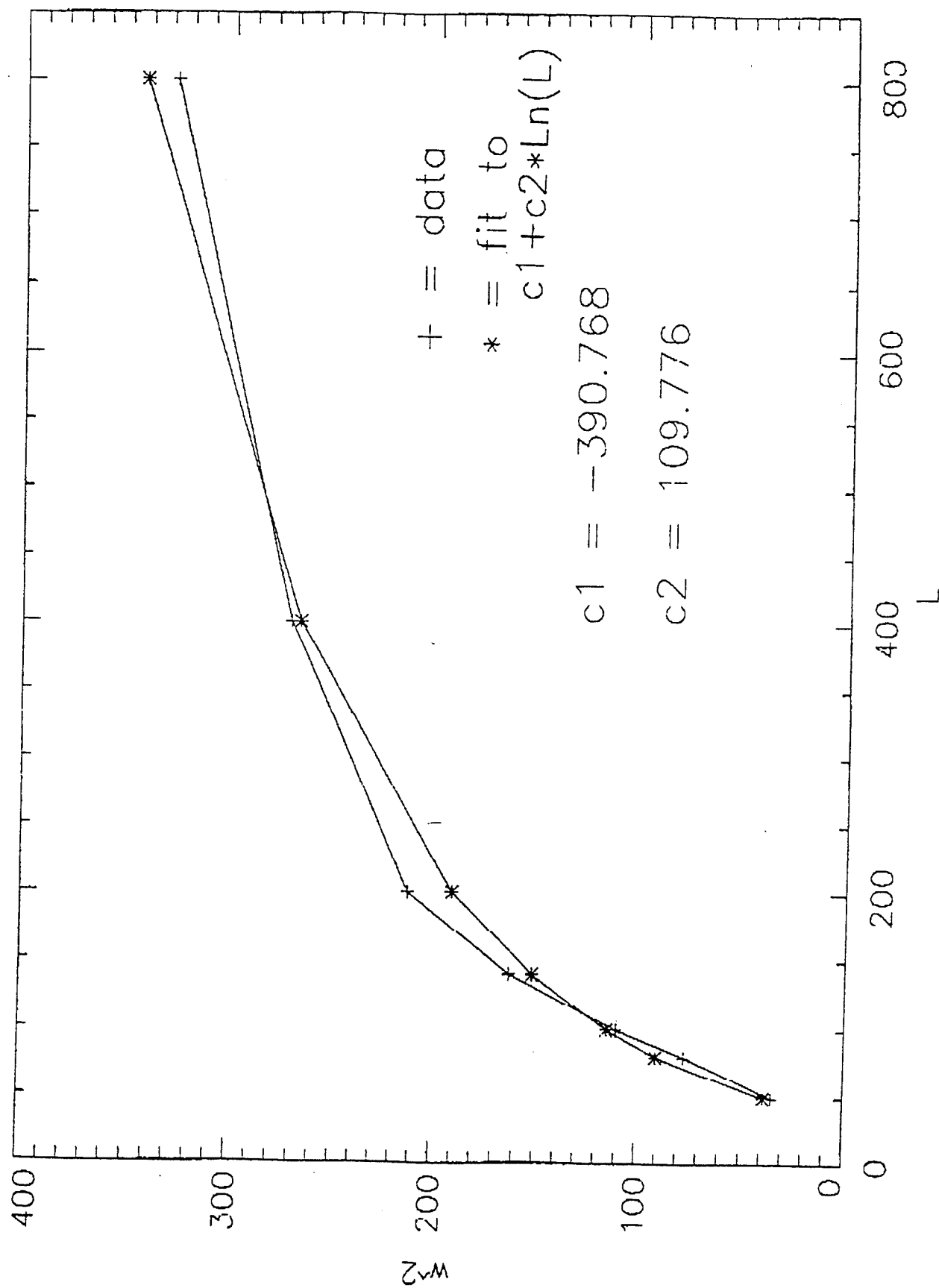
Fig 7
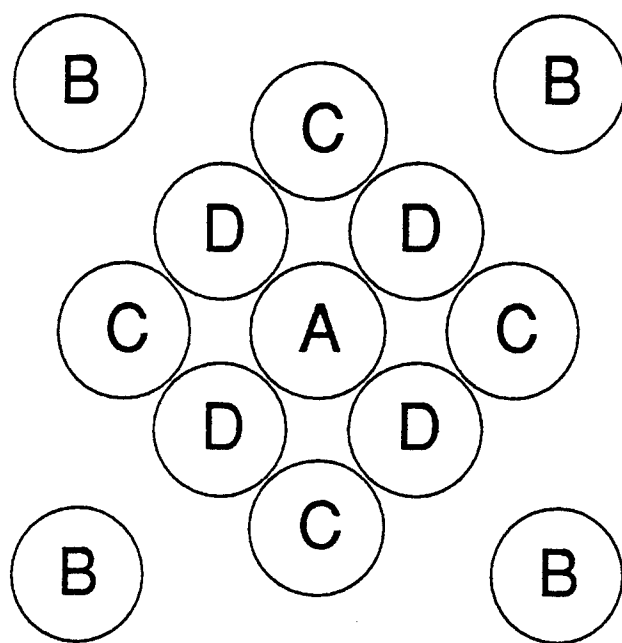
Fig. 8

Appendix A

ON THE POSSIBIITY OF CONVECTION IN THE 3M-PVTOS EXPERIMENT

ON THE POSSIBILITY OF CONVECTION
IN THE 3M-PVTOS EXPERIMENT

SHENG-NAN LAI

ABSTRACT

Inspired by the surprising results found by M. K. Debe *et al.* in their 3M-PVTOS experiments, this short report is a preliminary study to understand the claimed important fluid dynamics of physical vapor transport in a closed cylindrical ampoule. The purpose and design of the 3M-PVTOS experiment are briefly discussed. The primary features of films grown in microgravity environments and ground control films are presented. Based on the PVT parameters provided by M. K. Debe *et al.*, a crude estimate of the possibility of convection is made. Finally, a summary of two theoretical studies is presented.

1. INTRODUCTION

Physical vapor transport (PVT) is an experimental method for growing crystalline solids and films by gaseous diffusion. In the PVT process a material is sublimed, frequently into an inert buffer gas, and allowed to advect down a temperature gradient to a growth interface where the material recondenses. Growth of single crystals by PVT has been commonplace for years. In particular, vapor transport within a closed ampoule offers an experimental simplicity often used. The fluid dynamics involved in such a process is not necessarily simple, however. Buoyancy-driven convection may arise in ground-based PVT experiments, and its presence certainly affects the mass transport rate and temperature distribution which in turn affects the quality of crystals. When the buffer gas is introduced, either by thermal decomposition of the source material or by intentionally introduced inert gas, the interplay of convection and diffusion complicates the situation even more and makes the outcome of the experiment harder to control. Experiments in a microgravity environment offer an opportunity to further study the underlying mechanisms that are influenced by unit gravity.

In 1985, M. K. Debe and co-workers grew organic thin films of copper phthalocyanine[*] (CuPc) by PVT in both low earth orbit (LEO) on the Space Shuttle Orbiter and in the laboratory as ground controls. Follow M. K. Debe, we name the experiment PVTOS hereafter, for PVT of organic solids. After a complete characterization, M. K. Debe *et al.*, in a series of three papers,[1-3] reported that CuPc thin films grown in LEO environments, when compared to those of the ground control films, are optically more homogeneous and smoother, are significantly denser in their central portions, are more highly uniaxially oriented, and contain, essentially, a new crystalline polymorph different from those seen in ground control films. In order to give a satisfactory explanation to their surprising results, M. K. Debe *et al.* made a further analysis of the gas-phase evolution and convective heat transfer of their PVT experiments and concluded that, among other PVT parameters, the presence of *convection* in the ground-based PVT experiments and in the edge regions of the LEO experiments may

---

⋆ See Appendix A and Fig. A.1 for the chemical structure of the CuPc molecule.

2

be the primary feature causing the small variation among the ground control films and their larger distinctions from the LEO films.[†]

Inspired by their observations, our aim in this study is to understand the gas-phase behavior of the closed-cell PVT process including the possibility of natural convection (either thermal or solutal) and, if the convection exists, the flow pattern, the speed of the convection and the distribution of the temperature within the PVT ampoule. In particular, we would like to estimate (i) the rate of arrival of CuPc molecules, (ii) the speed of the wind of residual CuPc molecules and buffer gases sweeping across the growth interface, (iii) the temperature distribution on the growth interface. The hope is that through the understanding of this gas-phase behavior one can provide the appropriate microscopic boundary conditions on the gas-solid interface as an input for a computer simulation of the crystal growth. By this approach we wish to single out the most important parameters in the closed-cell PVT process and, hopefully, simulate the advantages, if any, of the microgravity environment in an earth-bound laboratory.

In this report, we first describe some of Debe's experimental results and his explanations of the surprising results (see also Appendix B.) By using the results of linear stability analysis of natural convection and its experimental verification, we next analyze the possibility of natural convection in Debe's PVT experiments. Then, a summary of two numerical studies in direct support of Debe's PVT experiments is presented. Table III and Appendix A present quantitative estimates of many of the physical parameters, macroscopic and microscopic needed in assessing aspects of the experiments or in setting up simulations. Finally, at the conclusion of this report, we comment briefly on future experiments.

---

† See the first paragraph of Sec. 5 on page 345 of Ref. 3.

2. DISCUSSION

The apparatus used by M. K. Debe *et al.* is schematically shown in Fig. 1. Fig. 2 is a cut-away view of the same apparatus. For a more detailed description of the design and performance Refs. 4 and 5 may be consulted. The PVT process occurs within the ampoule, which is a 1.7 cm diameter by 7.5 cm long Pyrex tube. The organic source material is confined to the hot end of the tube; the substrate platen, which is a 1.4 cm diameter copper disk, is at the cooler end. Outside the ampoule, there is an electrical heater wound with resistance wire used to maintain a non-linear axial temperature gradient between the hot end and the cool end of the ampoule. A heat pipe maintains the substrate temperature near 70° C; a computer-controlled heater kept the hot end of the ampoule at about 400° C for 4 hours during the PVT process. The ampoule and heater are placed concentrically into a cylindrical stainless steel cell which provides a vacuum envelope for the heater. At the beginning, the ampoules are filled with 550 mTorr He or 400 mTorr Xe and the cells, the region outside the ampoule but inside the stainless-steel cell (see Figs. 1 and 2), are evacuated. After the PVT process, the ampoules contain, mainly, the original buffer gas, plus H_2, CO_2 and CO (of total pressure about 3 Torr) which, except for the original buffer gas, are outgassed from the bulk of the glass and stainless-steel components inside the ampoule and formed from the decomposition of the CuPc source material. The cells' gas content after the PVT process, also due to outgassing, is primarily of H_2 with smaller amounts of several other common gases at total pressures on the order of one Torr.

Fig. 3 and Fig. 4 show the micrographs of a LEO sample and a ground control sample, respectively. The ground control sample G2, which by virtue of the PVT parameters used, has been considered by the authors the best ground control: G2 has almost the same PVT parameters as LEO1 has. They have the same initial buffer gas, Xe at 400 mTorr, the same final cell pressure, 0.4 Torr H_2, and both of them have their substrate platens coated with H_2Pc seed films. The main differences are the temperature of the substrate platens, 68° for LEO1, 77° for G2, and, of course, the presence or absence of gravity, the LEO1 sample was produced in the microgravity en-

4

vironment while G2 was made in the ground-based laboratory with the ampoule's hot end up. However, when one compares these two sets of micrographs, the distinctions between the LEO sample and G2 sample are obvious. Firstly, the central portions of the LEO film is denser than the central portion of the ground control film and their microstructures are also different in that region. Secondly, the edge region of the LEO film is similar to the edge region of the ground control film.

Being so similar in their PVT parameters used, the dramatic difference between the film grown in ground-based experiment and that of the LEO is striking. One possible cause of the difference, as strongly suggested by M. K. Debe *et al.*,[*] is buoyancy-driven convection. According to the authors, the radial variation of the morphology of the LEO films is the consequence of convection which is minimized over the centers of the LEO films while remaining significant at their edges where very strong thermal gradients persist between the platen edges and the ampoule walls: see Figs. 1 and 2. In the LEO film centers, where the convection is minimized, the film growth mechanism remains unchanged as the ampoule pressure increases and the film morphology continues to exhibit dense domains, resembling the base layer microstructure. On the edges of the LEO films, and in all regions of the ground control films, the onset of convection is believed to cause a significant change in the film growth mechanism, resulting in the observed discrete whiskered microstructure. Debe's main arguments identifying convection as the causative factor are presented in Appendix B in his own words.

Now buoyancy-driven convection is a result of imbalance of forces. The forces can be analyzed in the following way. Consider a bubble of warm fluid, of radius R, which moves upward with a constant speed v in a fluid where a constant linear temperature gradient is maintained. The bubble coming from the hotter region is now in a cooler environment with fluid density greater than the fluid density in the bubble. The difference in density gives rise to the Archimedean buoyancy force, $F_b \sim g \mid \delta\rho \mid R^3$. Defining $-\partial\rho/\rho\partial T = \alpha$ to be the thermal expansivity of the fluid, the buoyancy force

---

⋆ See the first paragraph of Sec. 5 starting at page 345 of Ref. 3.

can be written in terms of the temperature difference δT as $F_b \sim g\alpha\rho \mid \delta T \mid R^3$. The relaxation time of the bubble's temperature, due to heat diffusion, is $\tau \sim R^2/\kappa$, where κ is the thermal diffusivity of the fluid. This means that at a given time t the temperature within the bubble is about that of its surroundings at an earlier instant of time, $t - \tau$; so that at time t the temperature difference δT between the bubble and its neighborhood is $\delta T \sim \mid \nabla T \mid v\tau \sim \mid \nabla T \mid R^2 v/\kappa$, which yields the Archimedean buoyancy force $F_b \sim g\alpha\rho \mid \nabla T \mid R^5 v/\kappa$. The buoyancy force is opposed by viscous drag, F_d, which, in a first approximation, is of order $\eta R v$, where η is the dynamic viscosity of the fluid. Thus, the motionless steady state becomes unstable when the buoyancy force just overcomes the viscous drag. The ratio of buoyancy force to viscous drag is a dimensionless number called the Rayleigh number

$$\mathbf{Ra} = g\alpha \mid \nabla T \mid R^4/\nu\kappa, \tag{2.1}$$

where

$$\nu = \eta/\rho, \tag{2.2}$$

is the kinematic viscosity. The Rayleigh number increases with the size of the bubble; the instability should first appear for bubbles of maximum size, say the radius of the ampoule a, compatible with the boundaries of the container. With this rough argument we cannot, however, estimate quantitatively the value of the critical Rayleigh number for the onset of convection.[†] We merely single out which dimensionless combination of parameters is most relevant in the stability analysis.

An exact mathematical description of convection is very difficult and an exact solution is still lacking even for the simplest system undergoing vigorous convective motion. Various approximate methods do exist, which lead to an analysis of the

---

† If we use more accurate expressions for the Archimedean force, F_b, the relaxation time, τ, and the viscous drag, F_d: $F_b \simeq 4\pi g \mid \delta\rho \mid R^3/3$, $\tau \simeq R^2/4\kappa$, $F_d \simeq 6\pi\eta v R$, which is the Stokes' law, the condition for the onset of convection, $F_b/F_d \geq 1$, leads to $\mathbf{Ra} = g\alpha \mid \nabla T \mid R^4/\nu\kappa \geq 18$. However, we should not take the above heuristic argument too seriously. An instability criterion must be derived from a *global* consideration of the fluid, *i.e.* , the *overall* internal energy released by the buoyancy force must overcome the *total* energy dissipated by viscosity and thermal conductivity.

stability of various modes of motion in the fluid and hence to predictions of which modes are the most likely to be observed. The results are approximate, but in some instances the approximation is a close one. For a vertical cylindrical container with walls of *infinite thermal conductivity* and an aspect ratio $\gamma = L/a = 6$, convection was found experimentally to set in near $\mathbf{Ra}^* = 220 \pm 12$.[6] A theoretical study, assuming axisymmetry, gave $\mathbf{Ra}^* = 230$.[7] *Perfectly insulating lateral walls* reduce the threshold to $\mathbf{Ra}^* = 67.4$, according to theory.[8]

Based on the data provided by M. K. Debe *et al.*,[4] we estimate various thermophysical parameters in Appendix A. The Rayleigh number we obtain is $\mathbf{Ra} = (1.1 \pm 0.6) \times 10^{-2}$, far below the threshold apparently needed to cause a buoyant convection. Even if the sidewall temperature is approximately isothermal from the hot end to a distance (say, 0.1 of the ampoule's length) close to the cool end, near which the temperature drops rapidly and the convection is confined to that part of the ampoule, the estimated Rayleigh number would rise only to 0.11 ± 0.06, still well below the threshold.

Another consideration should be mentioned here, however. For a two-component fluid with molecular weights of the source material or solute significantly larger than that of the buffer gas or solvent, which is the case of Debe's experiments, *density gradients* due to the varying concentrations of the two components may result in convection. For example, with the hot end up, the upward movement of a fluid bubble carries it to a region of hotter and "saltier" (*i.e.* , higher solute concentration) environment. Suppose the temperature in the bubble is relatively quick to equilibrate with its surroundings while the solute concentration χ is significantly slower to do so. The bubble then finds itself at about the same temperature, but with less solute and therefore less density, than its neighborhood, and so the upward movement is reinforced by buoyancy furthering a convection. The relative importance of these effects is measured by another Rayleigh number, the so-called *solutal Rayleigh number*

$$\mathbf{Rs} = g\beta \mid \nabla\chi \mid a^4/\nu D_{AB}, \qquad (2.3)$$

where $\beta \equiv \partial\rho/\rho\partial\chi$. Clearly β plays the role of α while D_{AB}, the binary diffusion

coefficient, plays the role of κ in the thermal convection analysis. While the theoretical analysis of solutal convection in a closed cylindrical ampoule is not available, experimentally solutal convection was found to set in at $\mathbf{Rs} = 180 \pm 14$.[9]

By taking $\beta = 1$, which is a good approximation for a low concentration binary fluid, we find the solutal Rayleigh number in Appendix A to be $\mathbf{Rs} = (2.2 \pm 0.8) \times 10^{-4}$. With such a small solutal Rayleigh number, the solutal effect would seem to play an insignificant role in Debe's PVT experiments.

Dr. Chernov[*] pointed out that at the corner formed by two walls of different temperatures (the corner bound by the copper platen and the ampoule's side-wall of Debe's PVT experiment seems to be of this sort), thermal stress may lead to convection even though the Rayleigh numbers of the system are small. Unfortunately, we do not know how to estimate the importance of this effect.

Thermal creep is another possible source that drives convection. Along a non-isothermal wall there is a thin layer of fluid, called the Knudsen layer, of thickness a few mean free paths that moves from the cold to the hot region with the (z-component) velocity which can be expressed as:[10]

$$v \simeq 0.8\nu \frac{\partial \ln T}{\partial z}. \qquad (2.4)$$

In an ampoule used to grow CuPc, a typical set of parameters is $\nu \simeq 35 \text{ cm}^2/\text{sec}$, with a temperature difference of about $673 - 343 \text{ K} = 330 \text{ K}$ maintained over a side-wall length L of about 7.5 cm. Under these conditions the thermal creep velocity is nearly 2.4 cm/sec. It is claimed that this cold-to-hot flow along the side walls will correspond to a hot-to-cold *core* flow of comparable velocity, and will probably not be negligible compared to typical buoyancy-induced velocities (see Ref. 11, p.1762 first column.) Unfortunately, we do not know how to incorporate this effect into our analysis.

We conclude this section by stating that it is *not* convincing to say that there is a buoyancy-driven convection in Debe's PVT experiments. Furthermore, since the

---

[*] A. A. Chernov, private communication.

gravity is reduced dramatically to between 10^{-3} and 10^{-6} times the earth value of $g = 9.8$ m/s^2 in the microgravity environment, buoyant force is dramatically reduced, so is the chance of buoyancy-driven convection. Although one cannot exclude other possible sources of convection, it is beyond the powers of the author to establish their importance or unimportance.

3. REVIEW OF PREVIOUS NUMERICAL STUDIES

Many theoretical attempts have been made to understand the fluid dynamics in the closed-cell PVT process,[12-16] of which Ref. 15 by T. L. Miller and Ref. 16 by D. E. Rosner and D. E. Keyes are numerical studies in direct support of Debe's PVT experiments. In this section I shall summarize some of their results.

Using the notation set out in Table I (see page 29), Miller employed the following governing equations to explore the diversity of possible fluid dynamics with the PVT ampoule:

Conservation of radial momentum:

$$\frac{\partial v}{\partial t} = -\vec{V} \cdot \vec{\nabla} v - \frac{1}{\rho_0}\frac{\partial p}{\partial r} + \nu \left(\nabla^2 v - \frac{v}{r}\right), \tag{3.1}$$

Conservation of axial momentum:

$$\frac{\partial w}{\partial t} = -\vec{V} \cdot \vec{\nabla} w - \frac{1}{\rho_0}\frac{\partial p}{\partial z} + \nu\nabla^2 w - g\left(\frac{\rho}{\rho_0} - 1\right), \tag{3.2}$$

Conservation of internal energy:

$$\frac{\partial T}{\partial t} = -\vec{V} \cdot \vec{\nabla} T + \kappa\nabla^2 T, \tag{3.3}$$

Conservation of mass for component A:

$$\frac{\partial \chi}{\partial t} = -\vec{V} \cdot \vec{\nabla} \chi + D_{AB}\nabla^2 \chi, \tag{3.4}$$

where incompressibility: $\vec{\nabla} \cdot \vec{V} = 0$, and axisymmetry are assumed and the condition of conservation of total mass: $d\rho/dt = -\rho\vec{\nabla} \cdot \vec{V} = 0$, has already been embedded in

9

the above equations. The *constitutive relation* is taken as

$$\rho = \rho_0 \left[1 - \alpha(T - T_0) + \beta(\chi - \chi_0)\right]. \tag{3.5}$$

The boundary conditions on temperature are assumed constant on each of the end walls, while sidewalls are either adiabatic (*i.e.* insulating) or have a fixed temperature profile. Non-slip conditions on the boundaries are assumed for the tangential velocity components. Impervious sidewalls are assumed, and the end walls have the boundary condition on the axial velocity component:

$$w = -\frac{D_{AB}}{1 - \chi}\frac{\partial \chi}{\partial z}. \tag{3.6}$$

The reason that this particular form is used instead of

$$j = -\rho D_{AB}\frac{\partial \chi}{\partial z}, \tag{3.7}$$

is that the former is the mass average velocity relative to a *fixed* coordinate while the latter is the mass flux of component A relative to the mass average velocity of the whole fluid. For a full account, Ref. 17 may be consulted.

There exists an one-dimensional steady solution to these equations. If no variations in the radial direction are allowed (and the side-walls are ignored), the axial velocity, temperature, and solute profiles are given by:[15]

$$W = \frac{D_{AB}}{L}\log\left(\frac{1 - \chi_L}{1 - \chi_0}\right), \tag{3.8}$$

$$T(z) = \frac{T_L - T_0}{\exp\left(\frac{WL}{\kappa}\right) - 1}\left[\exp\left(\frac{Wz}{\kappa}\right) - 1\right] + T_0, \tag{3.9}$$

$$\chi(z) = \frac{\chi_L - \chi_0}{\exp\left(\frac{WL}{D_{AB}}\right) - 1}\left[\exp\left(\frac{Wz}{D_{AB}}\right) - 1\right] + \chi_0. \tag{3.10}$$

The axial velocity amplitude, W, is used as the velocity scale in defining many dimensionless parameters(see Table II). The one-dimensional solution is also used in computations as the initial state with which the ampoule system is marched forward numerically in time until a steady state solution is reached.

Before presenting Miller's computational results, a few points regarding the PVT parameters used by Miller must be mentioned:

(1) In general, the substrate acts as a sink for the source material. This will drive a mass flow, called the Stefan flow, toward the substrate platen. The Stefan flow is significant only when the partial pressure of the source material is larger or, at least, comparable to the partial pressure of the buffer gas. Miller did his simulations with the partial pressure of the source material larger than that of the buffer gas. However, the averaged partial pressure of CuPc vapor in Debe's experiments is about 10^{-4} Torr, which is much smaller than the buffer gas partial pressure, $\sim 4 - 8$ Torr.

(2) Given a small Rayleigh number of order 1/100 in the Debe's PVT experiments, absolutely no buoyant effect can be anticipated. Miller used a larger Rayleigh number of order of 1000 in his numerical simulation on the thermal convection for the purpose of illustration.

(3) In his simulation of the thermosolutal convection, Miller assumed that the diffusivity of the solute is much larger than that of heat. On the contrary, the actual thermal diffusivity, $\kappa = 113\,\mathrm{cm}^2/\mathrm{s}$ is much larger than the binary diffusion coefficient, $D_{AB} = 12.4\,\mathrm{cm}^2/\mathrm{s}$ in Debe's experiments (see Table III.)

Fig. 5 shows the computed effects of Peclet number, $\mathbf{Pe} = LW/D_{AB}$, on the mass profile on the crystal interface under zero gravity. The Peclet number is a measure of the relative strength of advective and diffusive fluxes. The mass flux is normalized to the standard one-dimensional flux used as starting condition. The effect is monotonic in $\mathbf{Pe}$, with increasing radial variation as the Peclet number increases. However, there is very little effect on the radially integrated mass flux.

Miller also did simulations on single-component fluids under unit gravity. He considered the case in which the ampoule is vertical, with the hot end down, and the density difference due to differing molecular weights of the material is negligible, that is, no solutal effects on the buoyancy are considered. Even though Miller noticed that "the actual physical parameters as estimated by Dr. Mark Debe of 3M result

THIS PAGE IS MISSING IN ORIGINAL DOCUMENT

12 — 13

APPENDIX A Determination of Physical
Parameters in Debe's Experiments

In the hope of getting a feeling for Debe's 3M PVTOS experiments on the one hand and providing basic information for computer simulations on the other, we estimate some useful thermophysical parameters in this appendix. Although Debe has given some parameters in one of his papers,[*] no uncertainties are quoted. This appendix is self-contained as regards references.

A. Some information about CuPc molecules

(A.1) Molecular structure of CuPc molecules

The formula for CuPc molecules is $CuPc = CuC_{32}N_8H_{16}$. As regards the molecular structure, please see Fig. A1.

(A.2) Molecular dimensions of CuPc molecules

The copper phthalocyanine (CuPc) is a rectangular-like molecule of dimensions $a \times a \times b$ with $a \simeq 10\mathring{A}$ and $b \simeq 3\mathring{A}$, where b is estimated from the interaction energy (see Fig. A2) between two CuPc molecules with one on top of the other.

(A.3) The crystalline structure of CuPc crystals

There are at least seven distinguishable crystalline polymorphs of CuPc. Figs. A3 and A4 present the most frequently encounted crystalline polymorphs of CuPc: $\alpha-$CuPc and $\beta-$CuPc.

B. Estimates of thermophysical parameters

The calculations are based on the following gas composition:

Species	y_i	M_i(g/mole)	σ_i(Å)	ϵ_i/k_B(K)	k_i(mW/cm·K)
H_2	0.375	2	2.827	59.7	2.65
CO	0.125	28	3.69	91.7	0.35
CO_2	0.375	44	3.941	195.2	0.322
Xe	0.125	131.3	4.047	231	0.087

[*] See M. K. Debe *et al., J. Vac. Sci. Technol.,* **A8** (1990)

14

where σ and ϵ/k_B are taken from Appendix B of R. C. Reid *et al.*, *The Properties of Gases and Liquids*, fourth edition (McGraw-Hill, New York 1987), p.733–734; k_i, the thermal conductivity, is taken from M. K. Debe *et al.*, *J. Vac. Sci. Technol.*, **A8** (1990), p.58. The total gas pressure is $p = 3.2$ Torr at $T = 300$K and the mean molecular weight is $\bar{M} \equiv \sum_i y_i M_i = 37.2$ g/mole.

(B.1) <u>Mean gas density, ρ</u>

$$\rho = n\bar{M}, \qquad \bar{M} = 37.2 \text{ g/mole} \simeq 6.2 \times 10^{-23} \text{ g}, \qquad (A.1)$$

$$n \equiv \frac{N}{V} = \frac{p}{k_B T}. \qquad (A.2)$$

At $T = 300\ ^\circ$K

$$p = 3.2 \text{ Torr} = (3.2 \text{ Torr})(1.33 \times 10^2 \text{ N/m}^2 \cdot \text{Torr}), \qquad (A.3)$$

$$n \simeq \frac{(3.2 \text{ Torr})(1.33 \times 10^2 \text{ N/m}^2 \cdot \text{Torr})}{(1.38 \times 10^{-23} \text{ J/K})(300 \text{ K})} \simeq 1.03 \times 10^{23} \text{ 1/m}^3$$

$$\simeq 1.03 \times 10^{17} \text{ 1/cm}^3, \qquad (A.4)$$

$$\rho = n\bar{M} \simeq (1.03 \times 10^{17} \text{ 1/cm}^3)(6.2 \times 10^{-23} \text{ g})$$

$$\simeq 6.4 \times 10^{-6} \text{ g/cm}^3, \qquad (A.5)$$

which agrees with what Debe obtained: 6.4×10^{-6} gm/cm^3.[†] Calculations of ρ from the partial pressure data given by M. K. Debe *et al.*(Figs. 5 and 6 of *J. Vac. Sci. Technol.*, **A8** (1990) p.49–60) show that ρ is between 6×10^{-6} g/cm^3 and 1×10^{-5} g/cm^3. Therefore, a reasonable estimate for ρ is

$$\rho = (8 \pm 2) \times 10^{-6} \text{ g/cm}^3. \qquad (A.6)$$

(B.2) <u>CuPc vapor pressure</u>

---

† See M. K. Debe *et al.*, *J. Vac. Sci. Technol.*, A 8, 1990, p.58, first column.

The CuPc vapor pressure can be obtained from the empirical formula[‡]

$$p = 760 \times 10^{(-A/T+B)} \text{ Torr}, \qquad (A.7)$$

where $A = 13661 \pm 253$ and $b = 14.315 \pm 0.367$. At the hot end where $T = 400\ °C = 673$ K, we have

$$p = \left(760 \times 10^{(-13661/673+14.315)} \pm \Delta\right) \text{ Torr}$$
$$\simeq (7.9 \times 10^{-4} \pm \Delta) \text{ Torr}, \qquad (A.8)$$
$$\Delta = (7.9 \times 10^{-4} \text{ Torr}) \left[(253)^2 (\ln 10/673)^2 + (0.367)^2(\ln 10)^2\right]^{1/2}$$
$$\simeq 9.5 \times 10^{-4} \text{ Torr}, \qquad (A.9)$$

$$p = (7.9 \pm 9.5) \times 10^{-4} \text{ Torr}. \qquad (A.10)$$

At the cold end where $T = 70°C = 343K$

$$p = \left(760 \times 10^{(-13661/343+14.315)} \pm \Delta\right) \text{ torr}$$
$$\simeq \left(2.3 \times 10^{-23} \pm \Delta\right) \text{ torr}, \qquad (A.11)$$
$$\Delta = \left(2.3 \times 10^{-23} \text{ Torr}\right) \left[(253)^2(\ln 10/343)^2 + (0.367)^2(\ln 10)^2\right]^{1/2}$$
$$\simeq 4.4 \times 10^{-23} \text{ Torr}, \qquad (A.12)$$

$$p = (2.3 \pm 4.4) \times 10^{-23} \text{ Torr}. \qquad (A.13)$$

By using the same formula, Debe obtains the vapor pressure of CuPc at $T = 400°$ C to be 3.8×10^{-3} Torr.[§]

(B.3) Mean free path of buffer gas and CuPc molecules.

[‡] See D. Bonderman *et al.*, *Journal of Chemical and Engineering Data*, **15** (3) (1970) p.399
[§] See M. K. Debe *et al.*, *J. Vac. Sci. Technol.*, A8, 1990, p.58, first column.

Using the formula for the mean free path, l:[¶]

$$l = \frac{\sqrt{\pi/8}}{n\sigma}, \qquad (A.14)$$

where n is the particle number density and σ is the cross section, and the ideal gas law:

$$p = nk_BT, \qquad (A.15)$$

we have

$$l = \sqrt{\frac{\pi}{8}} \frac{k_BT}{\sigma p}. \qquad (A.16)$$

Expressing T in K, p in Torr, σ in Å, l in cm, and substituting $k_B = 1.381 \times 10^{-23}$ Joule/°K, 1 Torr = 1 mmHg = $1/75.006$ N/cm^2, $1\text{Å} = 10^{-8}$ cm into Eq.(A.16), we have

$$l = \left(6.5 \times 10^{-4}\right)\frac{T}{\sigma p} \text{ cm.} \qquad (A.17)$$

For the buffer gas at $T = 500$ K, $p = 5$ Torr, $\sigma = 10$ Å, the mean free path between buffer gas is

$$l \simeq 6.5 \times 10^{-3} \text{ cm.} \qquad (A.18)$$

If there is no buffer gas, then at $T = 673$ K, $p = 7.9 \times 10^{-4}$ Torr, the mean free path between CuPc molecules is

$$l \simeq 11.1 \text{ cm,} \qquad (A.19)$$

where $\sigma = 50$ Å^2 is assumed. From eq.(A.18) and eq.(A.19), we conclude that CuPc molecules collide mostly with the buffer gas. If we take $p = p_{\text{buffer}} = 5$ Torr, $T = 500$ K, and $\sigma = 50$ Å^2, then the mean free path of a CuPc molecule is

$$l = 1.3 \times 10^{-3} \text{ cm.} \qquad (A.20)$$

Debe does not give estimates of the mean free path.

[¶] See Kerson Huang, *Statistical Mechanics*, second edition (John Wiley & Sons 1987), p.94, eq.(5.5)

(B.4) The rate of arrival/bombardment from vapor of CuPc on the surface

Assume: (i) mass transport by diffusion only, (ii) the buffer gas is stagnant. The mass flux of CuPc, j, satisfies the equation:

$$j = -\rho D_{AB} \frac{\partial \chi}{\partial z}, \qquad (A.21)$$

where χ is the fractional weight concentration of CuPc vapor, D_{AB} is the binary diffusion coefficient, and ρ is the mean density of the fluid. By definition, j is the mass flux of CuPc relative to the mass average velocity of the fluid. For a dilute system, $\chi \ll 1$, and since the buffer gas is stagnant, j can be regarded as the mass flux of CuPc relative to a fixed coordinate, *e.g.*, the ampoule. If we assume that ρ and D_{AB} are constant throughout the ampoule, then

$$\frac{\partial \chi}{\partial z} = -\frac{j}{\rho D_{AB}} = \text{constant}, \qquad (A.22)$$

where $j = $ const. is a consequence of conservation of mass. The solution to eq.(A.22) is

$$j = \rho D_{AB} \frac{\chi_L - \chi_0}{L} = D_{AB} \frac{\rho_{AL} - \rho_{A0}}{L}, \qquad (A.23)$$

where χ_L and χ_0 are the values of χ at the hot end and the cold end, respectively, and ρ_{AL} and ρ_{A0} are the density of CuPc at the hot end and cold end, respectively.

Using the formula

$$\rho_A = \frac{M_A p_A}{k_B T}, \qquad (A.24)$$

where $M_A = 575.67$ g/mole is the mass of CuPc molecules, p_A is the vapor pressure of CuPc, we have

$$\rho_{AL} \simeq 1.1 \times 10^{-8} \text{ g/cm}^3, \qquad (A.25)$$

$$\rho_{A0} \simeq 6.2 \times 10^{-28} \text{ g/cm}^3, \qquad (A.26)$$

and

$$j \simeq 1.8 \times 10^{-8} \text{ g/cm}^2 \cdot \text{s}. \qquad (A.27)$$

which compare well with what Debe obtained from the growth rate of the CuPc films.[*]

(B.5) <u>Kinematic viscosity, ν</u>

Using

(9-3.9)
$$\mu_i = \frac{26.69\sqrt{M_i T}}{\sigma_i^2 \Omega_i} \ \mu\text{Poise} \qquad (A.28)$$

(9-4.3)
$$\Omega_i = \frac{1.16145}{(T_i^*)^{0.14874}} + \frac{0.52487}{\exp(0.7732 T_i^*)} + \frac{2.16178}{\exp(2.4387 T_i^*)} \qquad (A.29)$$

(9-5.2)
$$\phi_{ij} = \frac{\left[1 + (\mu_i/\mu_j)^{1/2}(M_j/M_i)^{1/4}\right]^2}{[8(1 + M_i/M_j)]^{1/2}} \qquad (A.30)$$

(9-5.1)
$$\mu = \sum_{i=1}^{n} \left[y_i \mu_i \Big/ \sum_{j=1}^{n} y_j \phi_{ij} \right] \ \mu\text{Poise} \qquad (A.31)$$

where $T_i^* = T/(\epsilon_i/k_B)$. The above formulas are quoted from *The properties of Gases and Liquids*, 3rd edition by R. C. Reid *et al.*. The proceeding equation numbers are the equation numbers appearing in that book. At $T = (343 \text{ K} + 673 \text{ K})/2 = 508 \text{ K}$, the dynamical mixture viscosity is found to be $\mu \simeq 284 \ \mu\text{Poise}$. According to the book from which the above formula are quoted, errors seldom exceed 3 to 4 percent for the estimated value of μ. Therefore, a conservative estimate of μ is

$$\mu = 284(1 \pm 5\%) \ \mu\text{Poise} = 284 \pm 14 \ \mu\text{Poise}$$
$$= (284 \pm 14) \times 10^{-6} \text{ g/s} \cdot \text{cm}. \qquad (A.32)$$

The kinematic viscosity:

$$\nu = \frac{\mu}{\rho} = \frac{280 \times 10^{-6} \text{ g/s} \cdot \text{cm}}{8 \times 10^{-6} \text{ g/cm}^3} \pm \Delta = (35 \pm \Delta) \text{ cm}^2/\text{s}, \qquad (A.33)$$

---

[*] See M. K. Debe *et al.*, *J. Vac. Sci. Technol.*, A 8, 1990, p.58, near eq.(11).

$$\Delta = (35 \text{ cm}^3/\text{s}) \left[\left(\frac{14}{284} \right)^2 + \left(\frac{2}{8} \right) \right]^{1/2} \simeq 9 \text{cm}^2/\text{s}, \qquad (A.34)$$

$$\underline{\nu = (35 \pm 9) \text{ cm}^2/\text{s}.} \qquad (A.35)$$

this value is different from what Debe obtained: 130 cm^2/s.[*] The formulas Debe quoted for calculating thermophysical parameters are wrong or misprinted.[†]

(B.6) Thermal diffusivity, $\kappa = k/\rho c_p$

Using[*]

$$k = \sum_{i=1}^{n} \left[y_i k_i \bigg/ \sum_{j=1}^{n} y_j \phi_{ij} \right] \qquad (A.36)$$

and y_i, k_i given in table at the beginning of this appendix, the thermal conductivity of the gas mixture is

$$k \simeq 0.8 \text{ mW/cm} \cdot \text{K} \simeq 1.9 \times 10^{-4} \text{ cal/cm} \cdot \text{s} \cdot \text{K} \qquad (A.37)$$

The thermal conductivity we get is slightly larger than what Debe obtained: 1.6×10^{-4} cal/cm $\cdot$ s $\cdot$ K.[‡] Error is within 3%[§]. Therefore

$$k = 1.9 \times 10^{-4}(1 \pm 5\%) \text{ cal/cm} \cdot \text{s} \cdot \text{K}$$

---

[*] See M. K. Debe *et al.*, *J. Vac. Sci. Technol.*, **A** 8, 1990, p.59, second column. Debe uses the symbol η for the kinematic viscosity.

[†] In Ref. 4 p.58 Debe quoted

$$\Omega_i = \frac{1.16145}{T_i^*} + \frac{0.52487}{\exp(0.7732T_i^*)} + \frac{2.16178}{\exp(2.4387T_i^*)},$$

$$\phi_{ij} = \frac{\left[1 + (\mu_i/\mu_j)^{1/2}(M_j/M_i)^{1/4} \right]^2}{[8(1 + M_i/M_j)]}.$$

If the above formulas, instead of eqs. (A.29) and (A.30), are utilized, then $\nu = 437.64$ cm^2/s.

[*] See R. C. Reid *et al*, *The Properties of Gases and Liquids*, 3rd edition, Eq.(10–6.1)

[‡] See *J. Vac. Sci. Technol.*, A8(1990) p.59, 2nd column.

[§] See *The Properties of Gases and Liquids*, 3rd edition, p.512.

$$= (1.9 \pm 0.1) \times 10^{-4} \text{ cal/cm} \cdot \text{s} \cdot \text{K}. \qquad (A.38)$$

The averaged heat capacity per unit mass as given by M. K. Debe et $al.$[¶] is $c_p = 0.218 \text{ cal/g} \cdot \text{K}$. For an ideal gas with mass $\bar{M} = 37.2$ g/mole

$$c_p \simeq 3\,\text{R} \simeq 5.96 \text{ cal/mole} \cdot \text{K} \simeq 0.16 \text{ cal/g} \cdot \text{K} \qquad (A.39)$$

Therefore, a reasonable estimate for c_p is

$$c_p = (0.21 \pm 0.05) \text{ cal/g} \cdot \text{K}. \qquad (A.40)$$

For the thermal diffusivity we find

$$\kappa = \frac{k}{\rho c_p} = \frac{1.9 \times 10^{-4} \text{ cal/cm} \cdot \text{s} \cdot \text{K}}{(8 \times 10^{-6} \text{ g/cm}^3)(0.21 \text{ cal/g} \cdot \text{K})} \pm \Delta$$
$$\simeq (113 \pm \Delta) \text{ cm}^2/\text{s} \qquad (A.41)$$

$$\Delta = (113 \text{ cm}^2/\text{s}) \left[\left(\frac{0.1}{1.9} \right)^2 + \left(\frac{2}{8} \right)^2 + \left(\frac{0.05}{0.21} \right)^2 \right]^{1/2}$$
$$\simeq 39 \text{ cm}^2/\text{s}, \qquad (A.42)$$

$$\underline{\kappa = (113 \pm 39) \text{ cm}^2/\text{s}.} \qquad (A.43)$$

(B.7) Binary diffusion coefficient, $\underline{D_{AB}}$

The value for D_{AB} estimated by Debe, $D_{AB} = 12.4 \text{ cm}^2/\text{s}$, is subject to about 20% uncertainty:

$$D_{AB} \simeq 12.4(1 \pm 20\%) \text{ cm}^2/\text{s} \simeq (12.4 \pm 2.5) \text{ cm}^2/\text{s}, \qquad (A.44)$$

$$\underline{D_{AB} = (12.4 \pm 2.5) \text{ cm}^2/\text{s}.} \qquad (A.45)$$

(B.8) Thermal Rayleigh number, $\underline{\mathbf{Ra} = g\alpha \mid \nabla T \mid a^4/\nu\kappa}$

$$\mathbf{Ra} = \frac{\left(980 \text{ cm/s}^2 \right) \left(2 \times 10^{-3} \text{ 1/K} \right) (320 \text{ K}) (0.85 \text{ cm})^4}{(35 \text{ cm}^2/\text{s}) (113 \text{ cm}^2/\text{s}) (7.5 \text{ cm})} \pm \Delta$$

¶ See $J.$ $Vac.$ $Sci.$ $Technol.$, **A8**(1990) p.58.

21

$$\simeq 1.1 \times 10^{-2} \pm \Delta, \tag{A.46}$$

$$\Delta = (1.1 \times^{-2}) \left[\left(\frac{0.5}{2}\right)^2 + \left(\frac{10}{320}\right)^2 + 4\left(\frac{0.02}{0.85}\right)^2 + \left(\frac{9}{35}\right)^2 + \left(\frac{39}{113}\right)^2 + \left(\frac{0.1}{7.5}\right)^2 \right]^{1/2}$$

$$\simeq 0.6 \times 10^{-2}, \tag{A.47}$$

$$\underline{\mathbf{Ra} = (1.1 \pm 0.6) \times 10^{-2}.} \tag{A.48}$$

(B.9) <u>Solutal Rayleigh number, $\mathbf{Rs} = g\beta \mid \nabla\chi \mid a^4/\nu D_{AB}$</u>

By definition

$$\chi = \frac{\rho_A}{\rho_A + \rho_B} = \frac{\rho_A}{\rho}, \tag{A.49}$$

if we assume the ρ_B is constant, then

$$d\chi = \frac{\rho_B}{\rho^2}d\rho, \tag{A.50}$$

which leads to

$$\beta \equiv \frac{1}{\rho}\frac{\partial \rho}{\partial \chi} = \frac{1}{1-\chi}. \tag{A.51}$$

For a dilute system, $\chi \ll 1$, we may take $\beta = 1$, then the solutal Rayleigh number is

$$\mathbf{Rs} = \frac{\left(980 \text{ cm/s}^2\right)\left(1.4 \times 10^{-3}\right)(0.85 \text{ cm})^4}{(35 \text{ cm}^2/\text{s})\,(12.3 \text{ cm}^2/\text{s})\,(7.5 \text{ cm})} \pm \Delta$$

$$\simeq 2.2 \times 10^{-4} \pm \Delta, \tag{A.52}$$

$$\Delta = (2.22.2 \times^{-4}) \left[\left(\frac{0.2}{1.4}\right)^2 4\left(\frac{0.02}{0.85}\right)^2 + \left(\frac{9}{35}\right)^2 + \left(\frac{2.5}{12.3}\right)^2 + \left(\frac{0.1}{7.5}\right)^2 \right]^{1/2}$$

$$\simeq 0.8 \times 10^{-4}, \tag{A.53}$$

$$\underline{\mathbf{Rs} = (2.2 \pm 0.8) \times 10^{-4}.} \tag{A.54}$$

APPENDIX B.   Summary of Debe's Arguments for Convection

We summarize Debe's arguments for convecton in this appendix as a handy reference.

"The strong radial dependence of the LEO films' apparent color, ellipsometric response parameters and, most importantly, reflection spectra suggests that near the edges of those microgravity-grown films, the density is less than at their centers, while the lower density of the ground-control-grown films varies much less from one side of the film to the other. The fact that the optical properties of the edges of LEO films are the same as those of the unit-gravity-grown films provides a self-consistent argument that it is the absence of the convection at the centers of the LEO films which has produced the enhanced thin film properties described in this and the following two papers of this series, and not some other PVT parameter or experimental artifact." "In ref. 12 evidence was presented which indicated that, during the growth of the ground control films, there was more convective heat transferred to the substrate end of the ampoule when the ampoule was processed with its hotter end below its cooler end than vice versa. Also, those data indicated that more convective heat transfer occurred when the ampoule was processed with its hotter end up in unity gravity than when processed in LEO. These experimental observations are not unexpected given the strong radial thermal gradients known to exist between the edges of the sample substrate platens and the adjacent inside surface of the ampoule walls. Without further consideration of other transport mechanism differences occurring between microgravity and unit gravity, it would appear as though the presence of convection has affected the microstructure of the vapor-transport-grown films on a submicron scale which is microscopic compared with the size of classical convective cells." — From Ref. 1, sec. 5, p.286–287.

"The existence of the new polymorph is considered to be a consequence of both the closed-cell PVT processing and the epitaxial growth onto an oriented organic substrate film, but its exclusivity and high degree of crystallinity in the

microgravity-grown films are attributed to the absence of buoyancy-driven convecton which otherwise may disturb the delicate conditions required for epitaxy." — From Ref. 2, sec. 7, p.324.

"Scanning electron micrographs show that the film microstructure in the centers of the space-grown PVTOS CuPc is not only dramatically different from the ground controls, consistent with a new crystal form as claimed here, but also at least a factor of 2 denser. This enhanced density is seen to have a strong radial character over the diameter of the films, explaining the optical effects described in ref. 1 and attesting to the influence of thermal-gradient-driven convection on the microscopic physical structure of vapor-transport-grown films." — From Ref. 2, sec. 7, p.324.

"A second observation is that the parasitic CuPc wall deposition just above the platen (see Fig. 1 in ref. 1) seems to be related to the radial variation in the film areal density, mass per unit area, of the LEO films, but less often in the ground control films. The film areal densities are higher in the centers of the LEO films than the edges, suggesting that the wall deposition has lowered the volume density of the CuPc vapor immediately above the growth interface at the edges to below the volume density above the centers of the LEO films. For the same T_i at the center and edges, the supersaturation ratio of the CuPc vapor is thus higher at the center than at the edges of the LEO films. In the ground control films, the less obvious difference in areal mass density between centers and edges implies that convective mixing has lessened the variation in volume mass density of the CuPc vapor over the platen area, resulting in a more radially uniform S_r." — From Ref. 3, sec. 4.4, p.342.

"The substrate temperature increase is larger for higher ampoule pressures and hot-end-down runs, due to increased heat transfer from the ampoule's wall and hot-end to the substrate. This clearly indicates convection is contributing to the substrate temperature in the hot-end-down orientation, since thermal diffusion (Soret) effects are probably second order for heat transfer and not orientation

sensitive. Given the low Rayleigh number for this dilute system and ampoule aspect ratio, a one-dimensional axisymmetric linear stability model would not predict the existence of any free convection. It cannot be inferred however that there is convection in the hot-end-up orientation, cometimes referred to as the thermally stable configuration. Evidence that convection exists even in the hot-end-up orientation can be obtained by using the data of Figs. 7–9 to predict what the substrate temperatures of the microgravity processed substrates would have been had they been processed in unit gravity, and then showing that such temperatures are well above the actually observed substrate temperatures." — From Ref. 4, p.55–56.

REFERENCES

1. M. K. Debe, R. J. Poirer, D. D. Erickson, T. N. Tommet, D. R. Field and K. M. White, *Thin Solid Films* **186** (1990) 257.

2. M. K. Debe and K. K. Kam, *Thin Solid Films* **186** (1990) 289.

3. M. K. Debe and R. J. Poirer, *Thin Solid Films* **186** (1990) 326.

4. M. K. Debe, R. J. Poirer, E. L. Cook, L. R. Miller, M. S. Spiering and S. P. Floeder, *J. Vac. Sci. Technol.* **A8** (1) (1990) 49.

5. M. K. Debe, R. J. Poirer, F. S. Schroder, E. L. Cook, and G. J. Follet, *Rev. Sci. Instrum.* **61** (2) (1990) 865.

6. J. M. Olson and F. Rosenberger, *J. Fluid Mech.* **92** (1979) 609.

7. G. S. Charlson and R. L. Sani, *Int. J. Heat Mass Transfer* **14** (1971) 2157.

8. L. D. Landau and E. M. Lifshitz, *Fluid Mechanics* p.218.

9. J. M. Olson and F. Rosenberger, *J. Fluid Mech.* **92** (1979) 631.

10. M. N. Kogan, in *Annual Reviews of Fluid Mechanics* (Annual Reviews Inc., Palo Alto, CA, (1973)), Vol. 5, p.393, eq.(20).

11. D. E. Rosner, *Phys. Fluids* **A1** (1989) 1761.

12. D. W. Greenwell, B. L. Markham and F. Rosenberger, *J. Crystal Growth* **51** (1981) 413.

13. B. L. Markham, D. W. Greenwell and F. Rosenberger, *J. Crystal Growth* **51** (1981) 426.

14. A. Nadarajah and F. Rosenberger, *J. Crystal Growth* **51** (1981) 426.

15. T. L. Miller, *NASA Report* No. TP2620, 1986.

16. D. E. Rosner and D. E. Keyes, *NASA Report* No. CR185122, 1989.

17. F. Rosenberger, *Fundamentals of Crystal Growth I* (Springer, Berlin, 1979), p.232–233.

18. B. L. Stoddard, R. K. Strong, A. Arrott and G. K. Farber, *Nature* **360** (1992) 293.

TABLE I   List of Symbols Used

a Radius of ampoule.

D_{AB} Diffusivity of components A and B in the mixture.

g Gravitational acceleration.

k Thermal conductivity.

L Axial length of ampoule.

p Pressure within fluid.

q Heat current.

r Radial coordinate.

T_0 Temperature at $z = 0$, the cold end.

T_1, T_2 Other observed temperatures: see Fig. 1.

T_L Temperature at $z = L$, the hot end.

$\vec{V}$ Local velocity vector.

v, w Radial and axial velocity components, respectively.

W One-dimensional solution amplitude for axial velocity.

z Axial coordinate.

α Thermal expansivity.

β Solutal density factor.

η Dynamic viscosity.

κ Thermal diffusivity.

ν Kinematic viscosity.

ρ Fluid density.

ρ_0 Reference density.

χ Fractional weight concentration of component A (CuPc).

χ_0 Fractional weight concentration at $z = 0$, cold end.

χ_L Fractional weight concentration at $z = L$, hot end.

TABLE II   Definitions of Dimensionless Parameters

$\mathbf{Nu} = qL/k$ Nusselt number

$\mathbf{Pe} = LW/D_{AB}$ Solutal Péclet number

$\mathbf{Pe_t} = LW/\kappa$ Thermal Péclet number

$\mathbf{Pr} = \nu/\kappa$ Prandtl number

$\mathbf{Ra} = g\alpha(\nabla T)a^4/\nu\kappa$ Thermal Rayleigh number

$\mathbf{Re} = aW/\nu$ Reynolds number

$\mathbf{Rs} = g\beta(\nabla\chi)a^4/\nu D_{AB}$ Solutal Rayleigh number

$\mathbf{Sc} = \nu/D_{AB}$ Schmidt number

$\gamma = L/a$ Aspect ratio

TABLE III   Quantitative Features of Debe's Experiments

Average mixture kinematic viscosity[a] $\nu = (50 \pm 9)$ cm^2/s

Thermal diffusivity[a] $\kappa = (113 \pm 39)$ cm^2/s

Average heat capacity[b] $c_p = (0.21 \pm 0.05)$ cal/g $\cdot$ K

Binary diffusion coefficient[a] $D_{AB} = (12.4 \pm 2.5)$ cm^2/s

Effective CuPc vapor pressure at the growth interface[b] $p \simeq 10^{-7}$ Torr

Vapor pressure of CuPc at 400°C[a] $p \simeq 8 \times 10^{-4}$ Torr

Total gas pressure inside the ampoule[b] $p \simeq 4 \sim 8$ Torr

Temperature difference between hot end and cold end[b] $\Delta T = 335$ K

Total mean gas density[a] $\rho = (8 \pm 2) \times 10^{-6}$ g/cm^3

(a) See Appendix A.

(b) See M. K. Debe *et al.*, *J. Vac. Sci. Technol.*, **A8** (1990) 49.

FIGURE CAPTIONS

Fig. $A1$ Molecular structure of CuPc molecules. (After M. K. Debe *et al.*, Ref. 2.) on top of the other. (Communication from Mr. Da-Jiang Liu.)

Fig. $A2$ The interaction energy between two CuPc molecules with one on top of the other. (Communication from Mr. Da-Jiang Liu.)

Fig. $A3$ Crystal structure of α-CuPc. (Communication from Dr. Robin Selinger.)

Fig. $A4$ Crystal structure of β-CuPc. (After Dr. Robin Selinger.)

Fig. 1. Schematic diagram of the demountable PVTOS ampoule within its cell envelope, showing details of its internal components and the three temperatures measured, T_1 the hot end, T_2 the substrate, and T_3 the cell surface midpoint temperature. (After M. K. Debe *et al.*, Ref. 4.)

Fig. 2. Cut-away view of a PVTOS cell showing the internal heater and ampoule assembly used for physical vapor transport deposition of organic films in the Orbiter mid-deck. (After M. K. Debe *et al.*, *Rev. Sci. Instrum.*, **61** (1990) 865.)

Fig. 3. Scanning electron micrographs taken from the center of the microgravity grown film LEO2: (a) center,0°; (b), (c) center, 45°; (d) edge, 45°. (Magnifications, 30000×.) (After M. K. Debe *et al.*, Ref. 3.)

Fig. 4. Scanning electron micrograph from the ground control sample G2 from two viewing angles of the center and edge regions: (a) center, 45°; (b) center, 45°; (c) edge, 45°; (d) edge, 0°. (Magnifications: (a), (b), (d) 30000×; (c) 10000×.) (After M. K. Debe *et al.*, Ref. 3.)

Fig. 5. Normalized mass flux on the crystal interface as a function of radial distance from the sidewall for varying **Pe** and for fixed $\gamma = 1$, **Sc** $= 1$, and **Pr** $= 1$,and for no gravity. (a) **Pe** $= 5.29$, (b) **Pe** $= 4.37$, (c) **Pe** $= 2.74$, (b) **Pe** $= 2.20$, (b) **Pe** $= 0.94$. (After T. L. Miller, *NASA Technical Paper* **2620**.)

Fig. 6. Nusselt number (dimensionless heat flux) as a function of thermal Rayleigh number (zero solutal Ra) for the cases of **Pe** = 0 (no crystal growth) and **Pe** = 2.2, and for aspect ratio $\gamma = 1$. (After T. L. Miller, *NASA Technical Paper* **2620**.)

Fig. 7. Temperature and stream function contours for the case with the hot end down and buoyancy effects of a heavy component A included as well as those due to temperature. The parameters used are: aspect ratio $\gamma = 2$, **Pr** = 1, **Sc** = 0.1, **Pe** = 1, **Ra** = 3484, **Rs** = −1742. (After T. L. Miller, *NASA Technical Paper* **2620**.)

Fig. 8. As in Fig. 7, but for **Ra** = −1742 and **Rs** = 6969 (cold end down). (After T. L. Miller, *NASA Technical Paper* **2620**.)

Fig. 9. Grid, temperature contours $T = 510(10)673$ K and CuPc vapor contours $\chi = 1.24 \times 10^{-9}(10^{-4})3.82 \times 10^{-3}$ at standard operating conditions (3.2 Torr). (After D. E. Rosner and D. E. Keyes, *NASA Contractor Report* **185122**.)

Fig. 10. Grid, temperature contours $T = 510(10)673$ K and CuPc vapor contours $\chi = 1.24 \times 10^{-9}(10^{-4})3.82 \times 10^{-3}$ at standard operating conditions with parasitic heat loss. (After D. E. Rosner and D. E. Keyes, *NASA Contractor Report* **185122**.)

Fig. 11. Grid, temperature contours $T = 510(10)673$ K and CuPc vapor contours $\chi = 1.24 \times 10^{-9}(10^{-4})3.82 \times 10^{-3}$ at standard operating conditions with parasitic heat loss and equalibrium vapor boundary conditions on the side-walls. (After D. E. Rosner and D. E. Keyes, *NASA Contractor Report* **185122**.)

Fig. 12. Grid, stream function contours, vorticity contours, temperature contours $T = 510(10)673$ K and CuPc vapor contours $\chi = 1.24 \times 10^{-9}(10^{-4})3.82 \times 10^{-3}$ at $p_0 = 3.2 \times 10^3$ Torr(= 4.2 atm). (After D. E. Rosner and D. E. Keyes, *NASA Contractor Report* **185122**.)

Fig. A1

Fig. A2

34
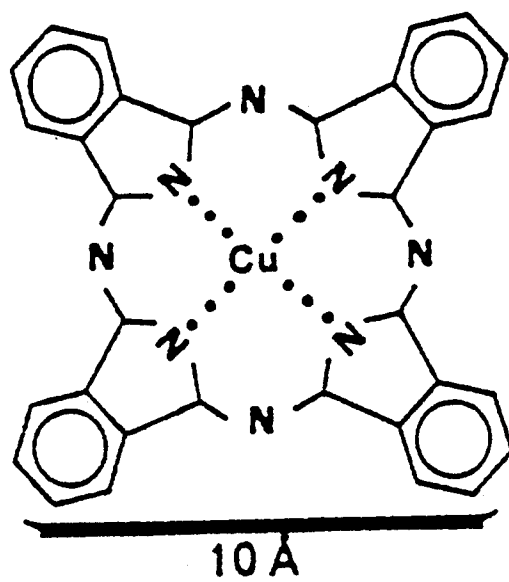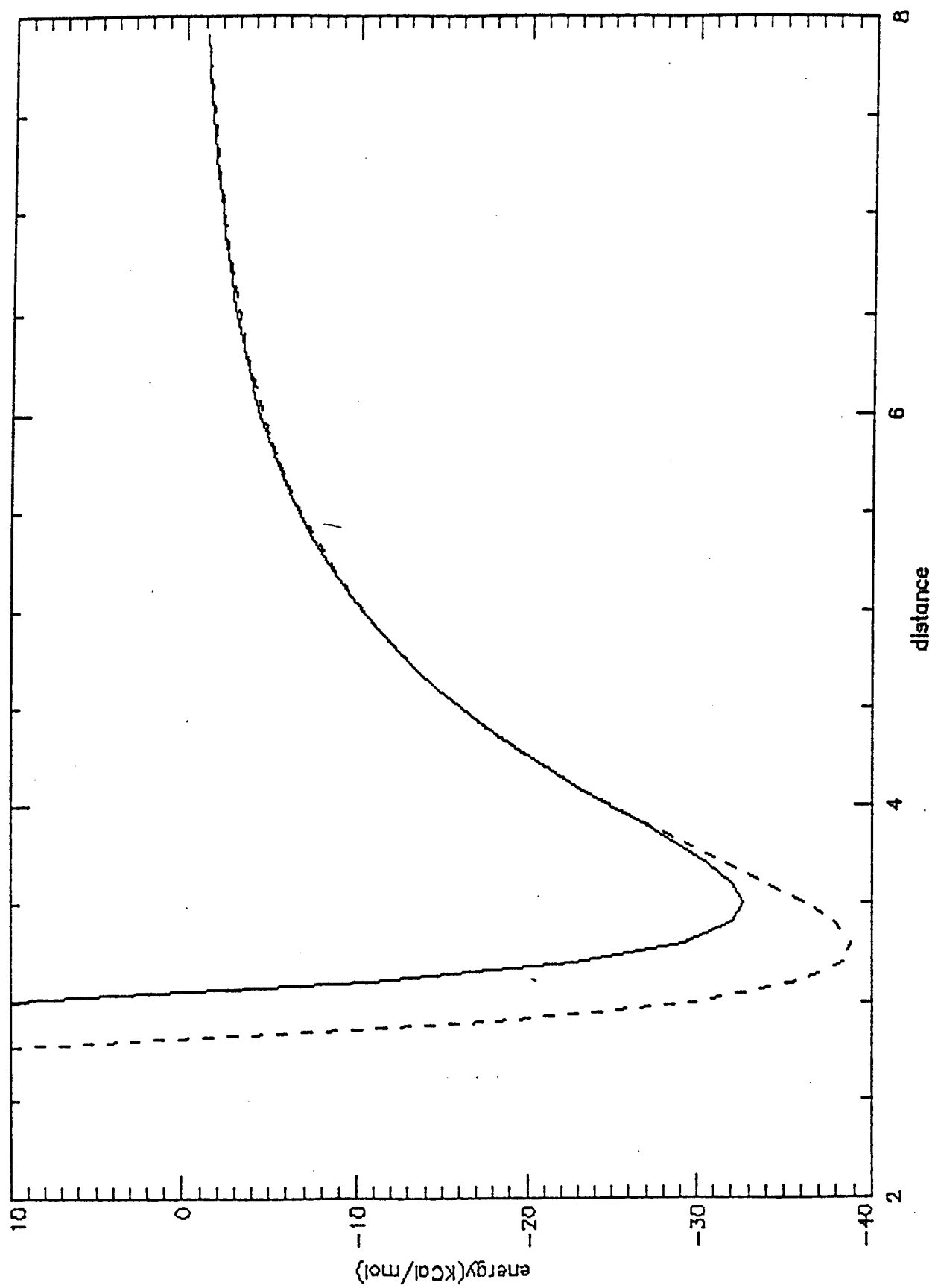
alpha-CuPc

C2/C

$a = 25.92$Å $b = 3.790$Å
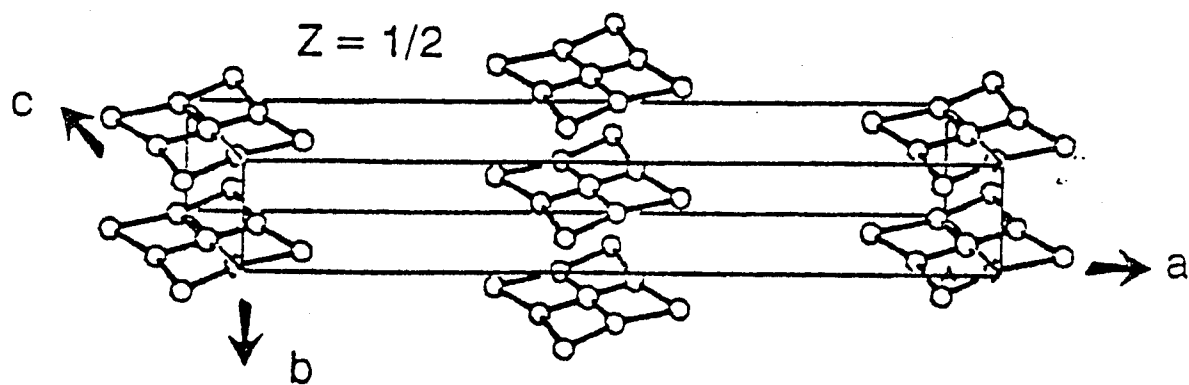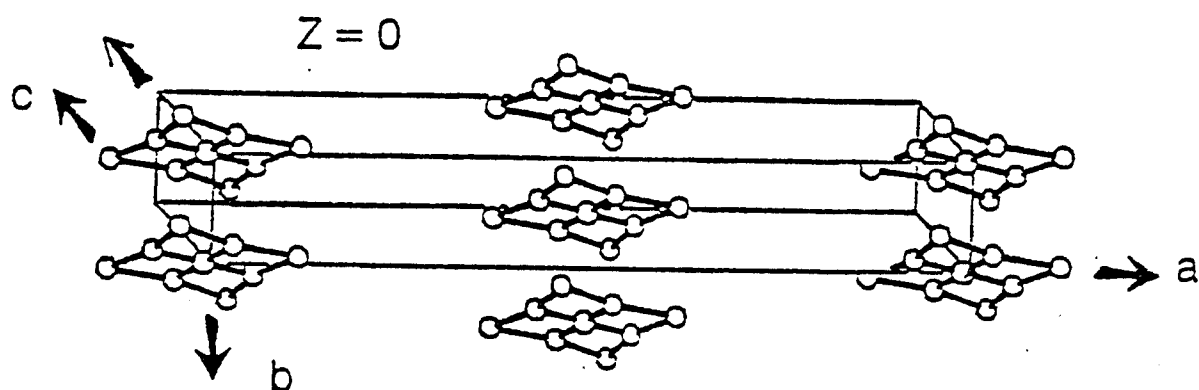
$c = 23.92$Å $\beta = 90.4$ deg.

Z = 0

Z = 1/2

ab projection

Fig. A3
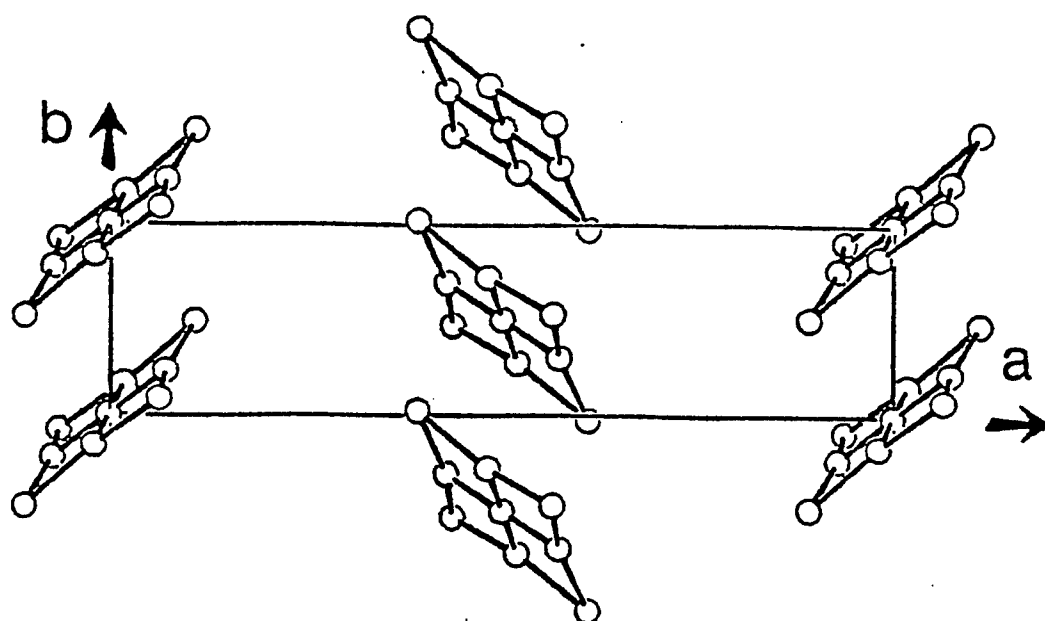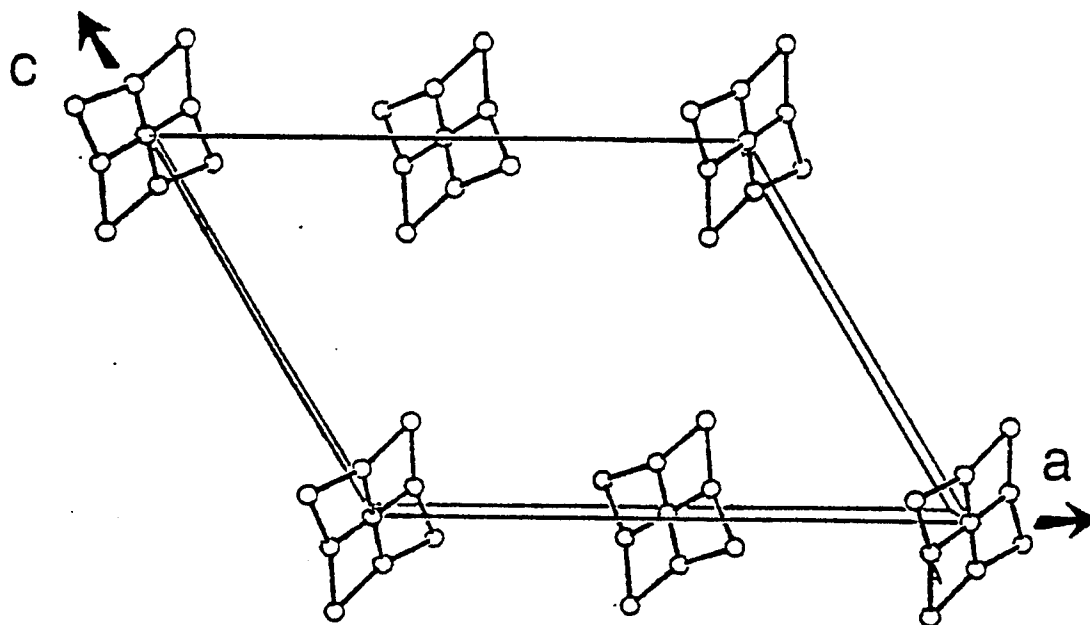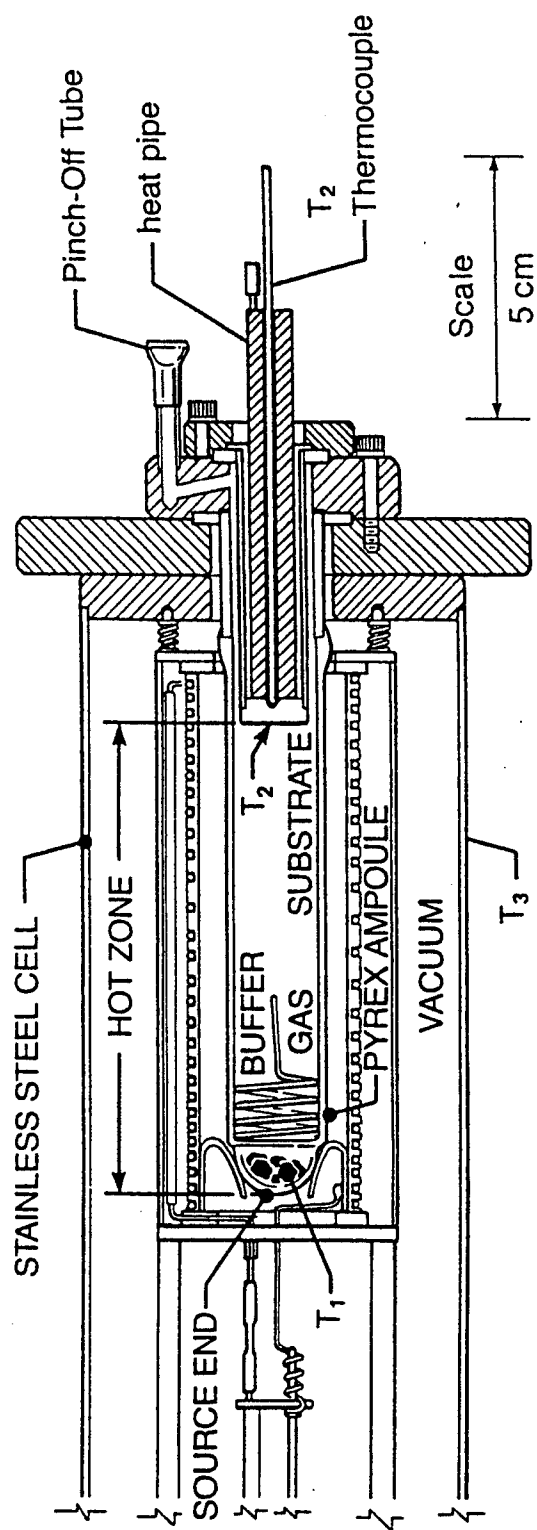
β -CuPc

P2$_1$/a

a = 19.407Å b = 4.790Å

c = 14.628Å β = 120.93 deg.

Fig. A4

Fig. 1
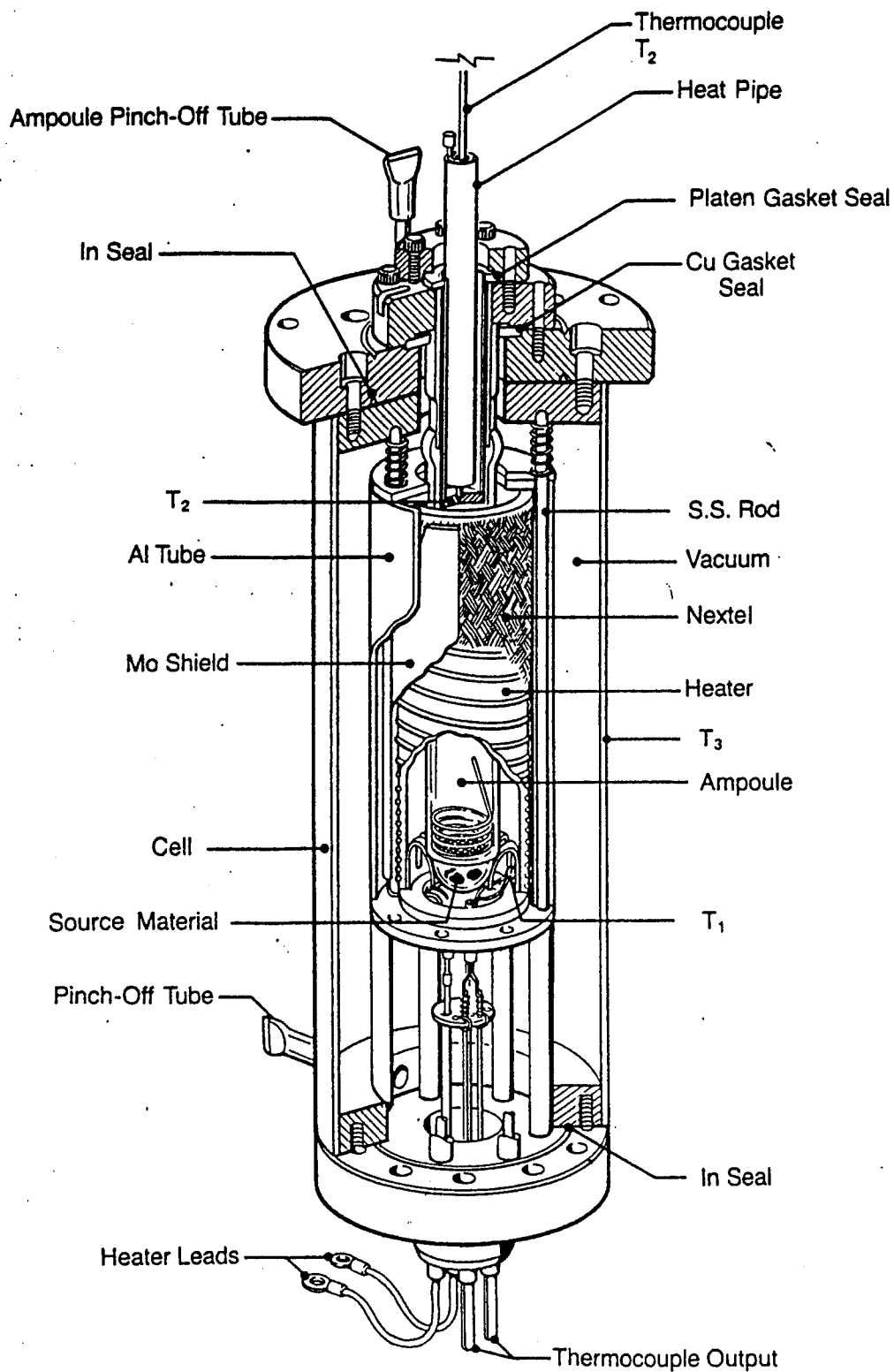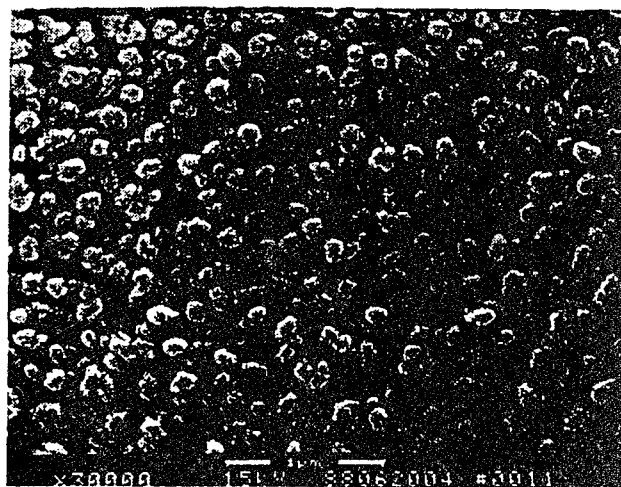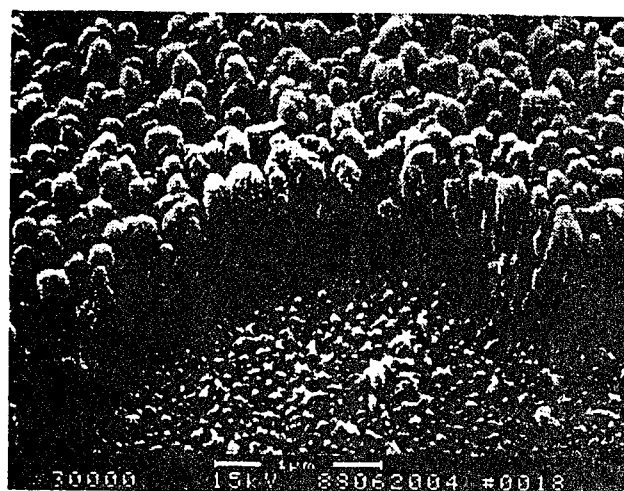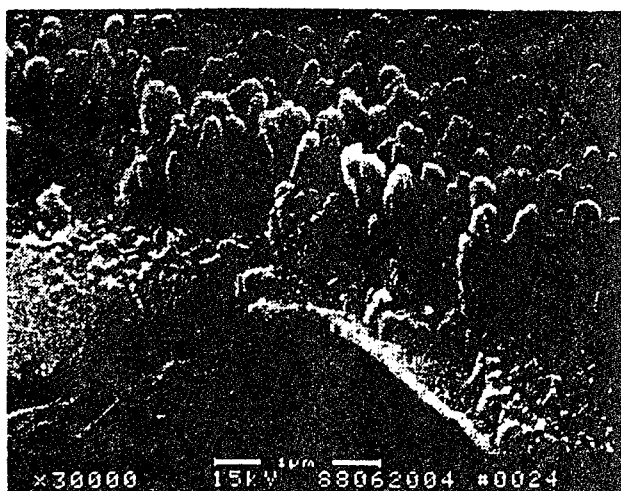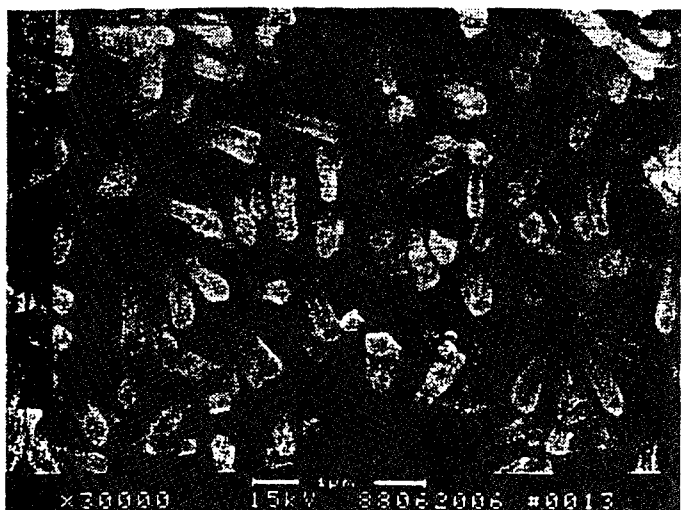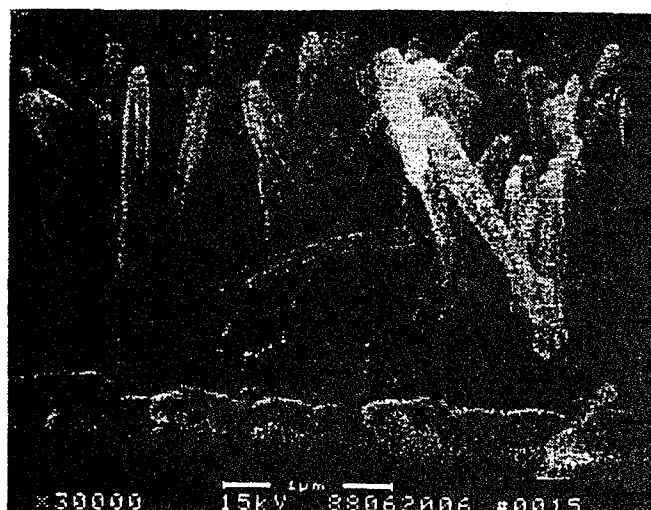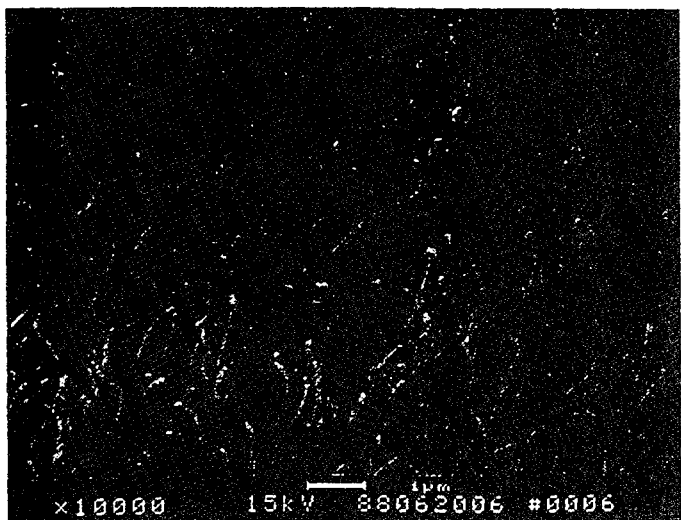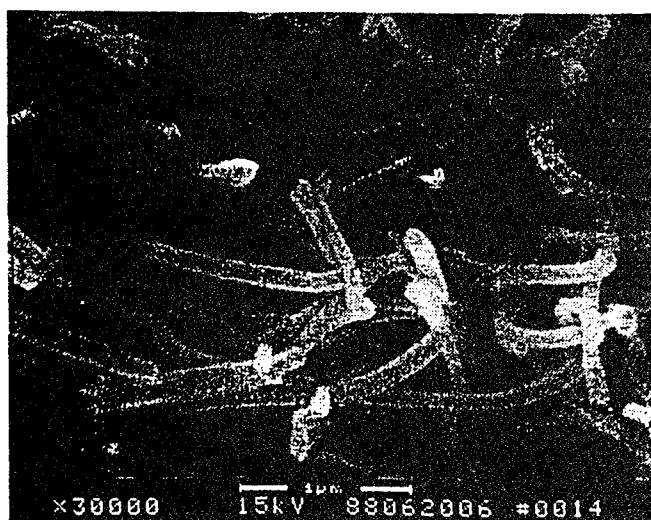
Thermocouple T_2

Ampoule Pinch-Off Tube

Heat Pipe

Platen Gasket Seal

In Seal

Cu Gasket Seal

T_2

S.S. Rod

Al Tube

Vacuum

Nextel

Mo Shield

Heater

T_3

Ampoule

Cell

Source Material

T_1

Pinch-Off Tube

In Seal

Heater Leads

Thermocouple Output

Fig. 2

38

(a)

(b)

(c)

(d)

Fig. 3

39

(a)

(b)

(c)

(d)

Fig. 4

Fig. 5

Fig. 6

41

Hot end

Cold end

TEMPERATURE
CONTOUR INTERVAL = 0.1000

STREAM FUNCTION
CONTOUR INTERVAL = 0.2000

↑g

Fig. 7

Hot end

Cold end

TEMPERATURE
CONTOUR INTERVAL = 0.1000

STREAM FUNCTION
CONTOUR INTERVAL = 0.2000

↓g
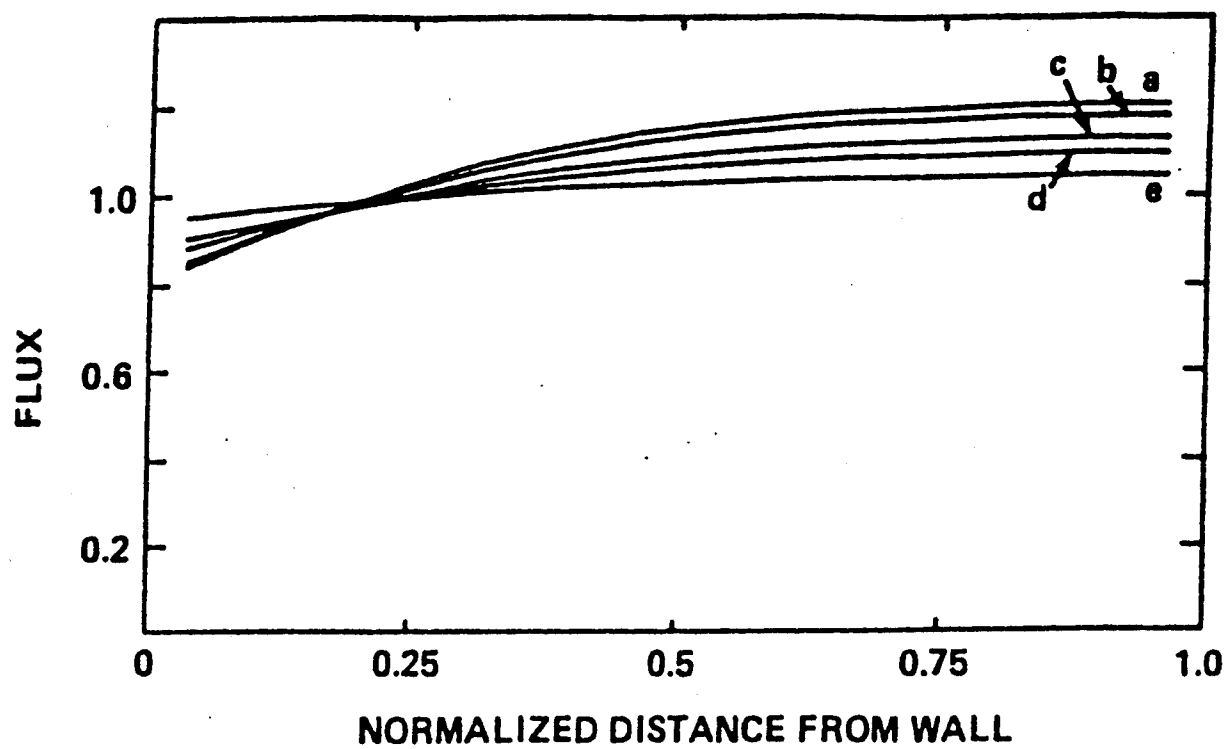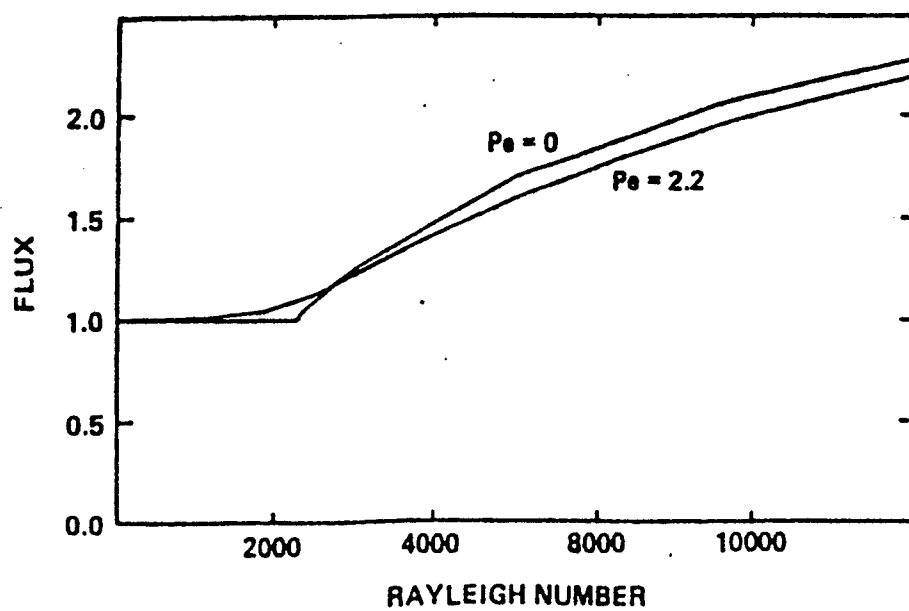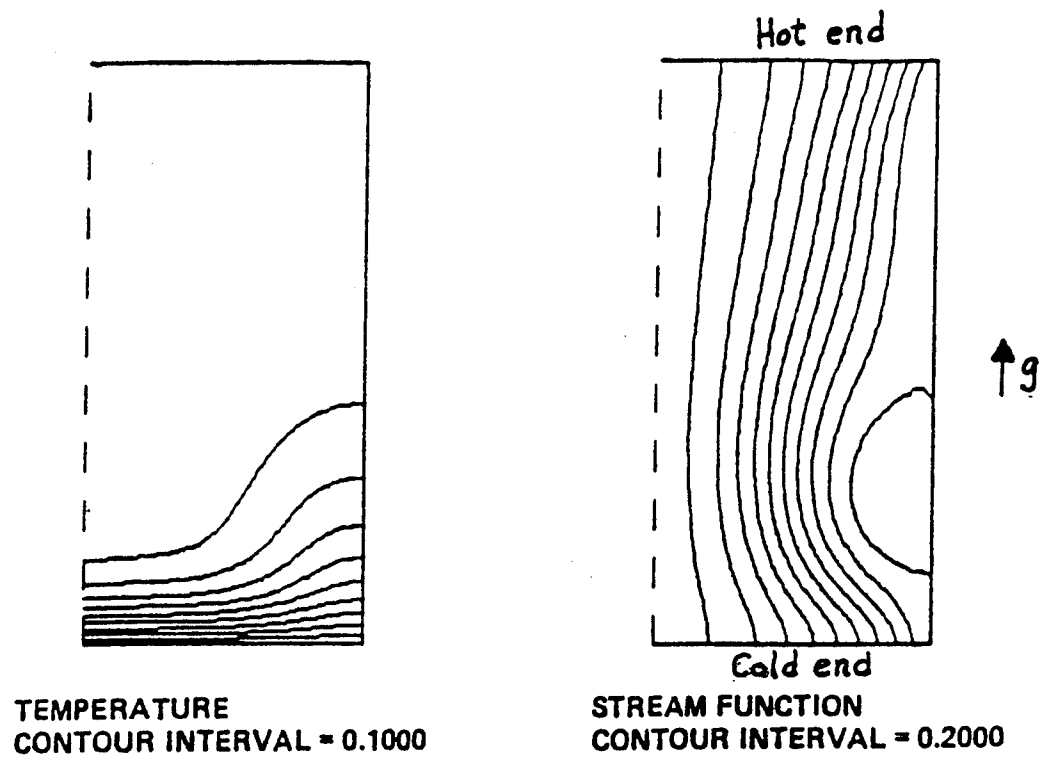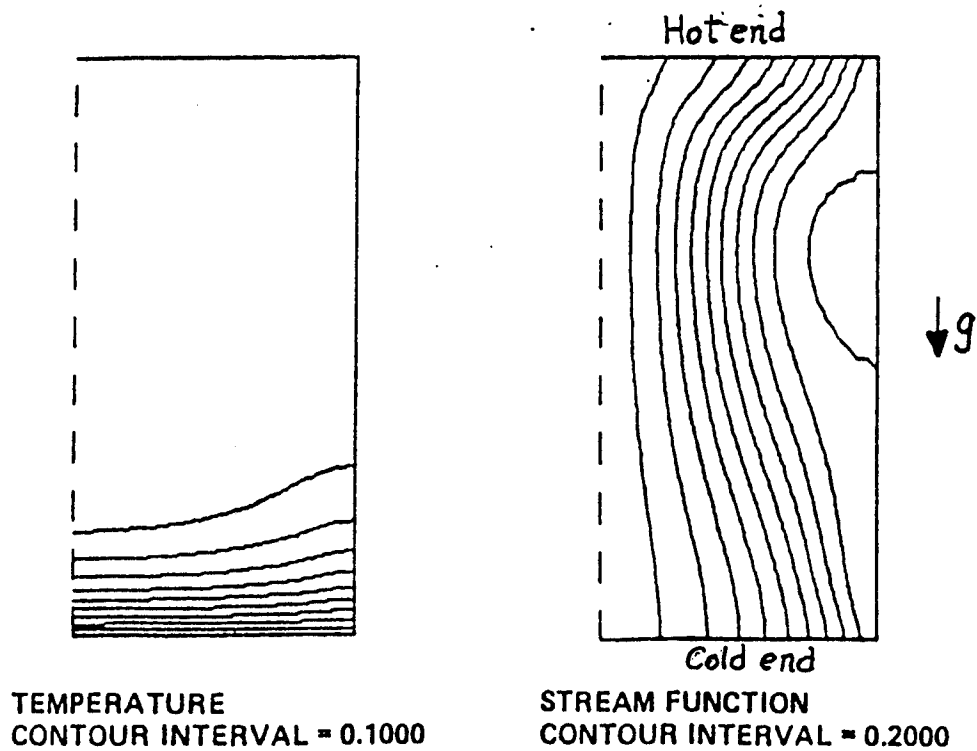
Fig. 8
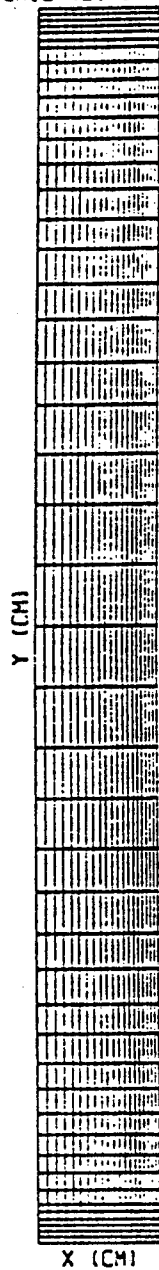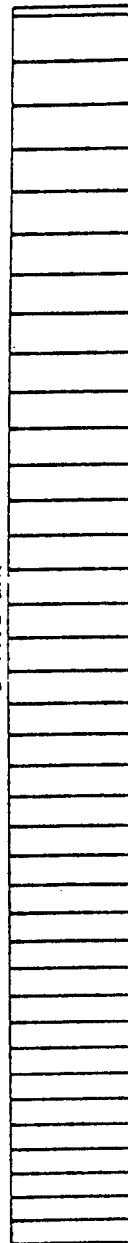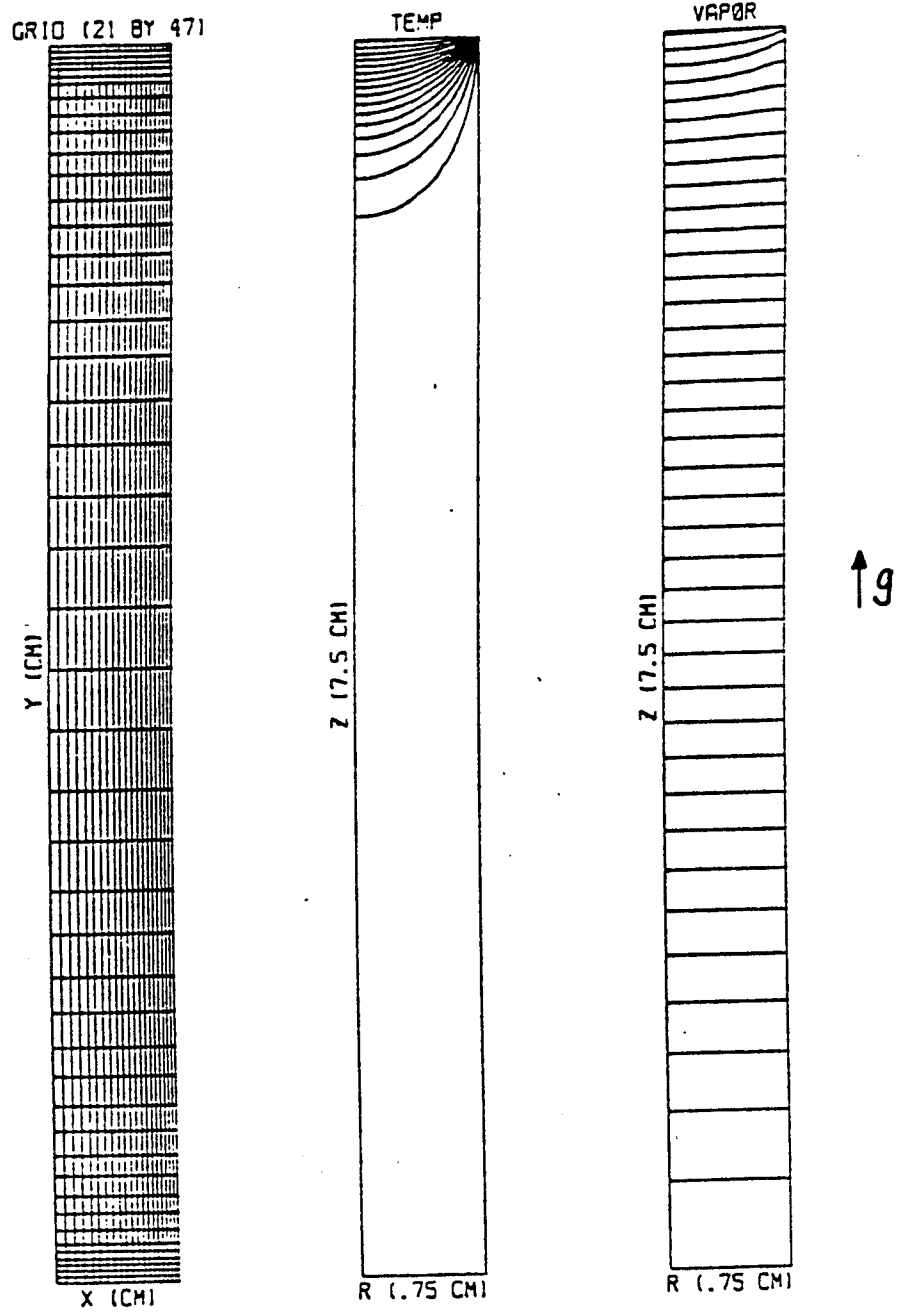
GRID (21 BY 47)   TEMP   VAPOR

Y (CM)   X (CM)   Z (7.5 CM)   R (.75 CM)   Z (7.5 CM)   R (.75 CM)   ↑g

Fig. 9

43

Fig. 10
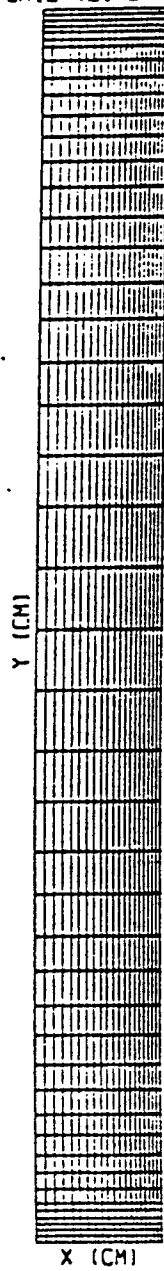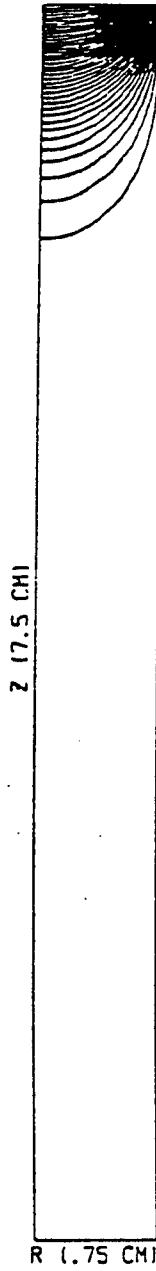
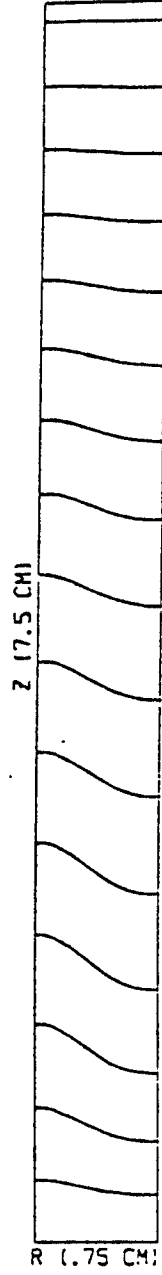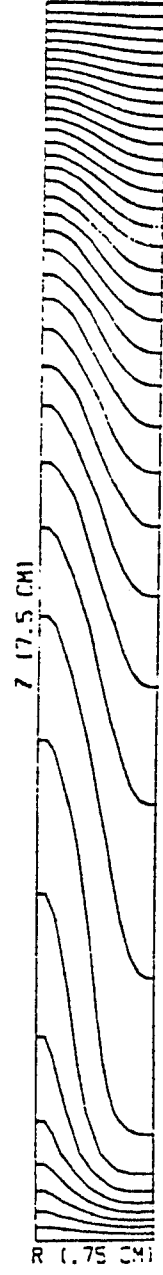Fig. 11
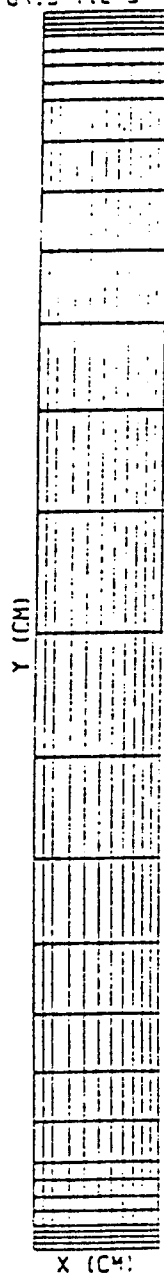
Fig. 12

Appendix B

MODELING ORGANIC MOLECULAR THIN FILMS: A REDUCED
INTERMOLECULAR POTENTIAL FOR COPPER PHTHALOCYANINE

Modelling Organic Molecular Thin Films: A Reduced Intermolecular Potential for Copper Phthalocyanine

Da-Jiang Liu, Robin L. Blumberg Selinger and John D. Weeks

Institute for Physical Science and Technology, University of Maryland, College Park, MD 20742

(August 9, 1994)

Abstract

The intermolecular potential energy between two molecules is often represented as a sum of spherically symmetric atomic potentials between all pairs of atoms on each molecule. While such potentials encode much physical and chemical information, the number of terms that must be summed over goes as the square of the number of atoms in a molecule; this inefficiency restricts the use of these potentials in computer simulation and modeling of large molecules. Starting with such an atomistic potential for Copper Phthalocyanine (CuPc), a molecule with 57 atoms, we determine a simpler reduced intermolecular potential consisting of a sum of effective pair interactions between a much smaller number of appropriately chosen "interaction sites" on each molecule. Some of the general issues and physical considerations that arise when attempting this reduction are discussed. We arrive at an effective potential involving 13 interaction sites in each molecule. This potential reproduces many qualitative features of the full atomistic potential model for CuPc but is much easier to evaluate numerically, requiring only 1% as much computation time as the full atomistic potential. Crystal structures of CuPc using both the atomistic and reduced potentials are determined and compared. Other possible applications of these ideas are discussed.

I. INTRODUCTION

The structure and properties of crystalline thin films of Copper Phthalocyanine (CuPc) have been the subject of much investigation[1,2] due to this material's potential applications in both solar energy conversion[3] and gas sensing[4]. When grown from the vapor phase, these thin films show a wide variation of morphology under changes in growth conditions[5]. Sensitive dependence of morphology on growth conditions such as substrate temperature has been observed in thin films of other organic materials as well[6].

The microscopic growth mechanisms which determine the structure and properties of organic crystalline thin films are poorly understood. One might expect that in the case of CuPc the planar, "tile-shaped" character of the individual molecules plays an important role at the microscopic level. The CuPc molecule has a nearly square, flat structure with a side length of approximately 10 Å and a thickness of about 3.5 Å , as shown in Fig. 1. During crystal growth from the vapor phase, the fundamental processes of surface diffusion and attachment of such anisotropic molecules could differ significantly from those observed in simpler materials, i.e. metal on metal epitaxial growth[7]. In order to make progress in understanding these microscopic aspects of crystal growth of CuPc, we must first find an intermolecular potential function, which is simply the energy of interaction between two molecules as a function of their relative separation and orientation. Through its dependence on relative orientation, the potential will implicitly include detailed information about the molecule's planar shape. The potential must be efficient enough in computation time to be useful for modelling applications.

An atomistic intermolecular potential for CuPc consisting of a sum of pair potentials for all constituent atoms was developed by A. Pohorille[8] using potential functions and parameters given in the CHARMM molecular modelling software package[9]. Pohorille adjusted some of the relevant parameters—the partial charges within the CuPc molecule—in order to achieve good agreement between the potential and the known crystal structure of β-CuPc. As discussed below, such a potential includes $N \times N$ pairwise interactions where N is the

2

number of atoms in a molecule; $N = 57$ for CuPc. Thus the determination of the interaction energy between just two molecules requires the calculation and summation of $57 \times 57 = 3249$ separate pair interaction functions. Such a potential requires too much computation time to be useful for modelling applications involving more than a few molecules. A look-up table is not a practical option because of the large number of degrees of freedom; storage requirements for the tabulated values would be too large.

Of course, even this atomistic representation of the interaction is only an approximation. Experience with such model potentials suggests that they are capable of providing an accurate representation of many qualitative and large-scale features of the true intermolecular interactions, particularly in a case like this where no strong intermolecular bonds are formed and the main attractive interaction is due to van der Waals forces. However it is unlikely that the fine details of the inherently quantum mechanical interactions are correctly described using a simple classical pairwise additive model potential.

The question we address here is: can we derive a "reduced" intermolecular potential for CuPc which reproduces these (presumably correct) large-scale features of the full atomistic intermolecular potential, yet is computationally efficient enough to use for large-scale simulation and modelling? We have chosen an approach in which the atomistic representation of the CuPc molecule is replaced by a relatively small number of "interaction sites", which can be thought of as representing groups of atoms in the original molecule. The reduced intermolecular potential is calculated as a sum of pair potentials summed over all pairs of interaction sites. The individual pair potentials for different species of interaction sites are parameterized in the Lennard-Jones 6-12 form, with parameters fitted to reproduce as closely as possible important features of the full atomistic intermolecular potential. In this way, we were able to determine a reduced potential which reproduces the gross features of the atomistic potential, yet requires *only 1% as much computation time.*

An alternative approach is to represent the molecular interaction as a single site-site potential function which depends explicitly on the center-to-center separation between molecules and their relative orientation. This approach was first proposed by Corner[10].

3

Gay and Berne[11] showed that for a rigid linear molecule consisting of four Lennard-Jones particles, the 16 atom-atom pair interactions could be well represented by a single site-site potential defined as the overlap between ellipsoidal Gaussian functions centered on each molecule. Their method was based on earlier work by Berne and Pechukas[12], and can be used to model molecules with shapes in the form of ellipsoids, both prolate and oblate. The Gaussian overlap potential has the advantage of being easily calculated and differentiated. But the CuPc molecule cannot be well approximated as a disk-like ellipsoid; as shown in Fig. 1, it has a nearly constant thickness and a definite four-fold symmetry that we expect plays an important role in determining crystal structure. As an alternative to our interaction site model one could attempt to formulate a more complicated single site-site potential by adding four-fold symmetric terms to the Gaussian overlap model. However such a modification might well compromise the model's main strengths of being easily calculated and differentiated.

It is difficult, though not impossible, to construct a more general single site-site potential for a rigid molecule whose shape is arbitrary; the Gaussian overlap model is only one example of many possible functional forms. Another choice would be to describe the CuPc molecule as, say, a tile-shaped hard core plus attractive forces. However the implementation of such a potential in a modelling application may prove difficult for other reasons. For instance, the use of a non-spherical hard potential in a Monte Carlo simulation requires a significant amount of computer time to test for the presence of particle overlaps in trial moves. Even for a soft potential written as an explicit function of molecular separation and relative orientation, some geometry calculations are required to determine the relevant angles and distances. While we have not fully explored the option of constructing a single site-site potential, we believe that the inherent simplicity of the interaction-site reduced potential makes it a better choice for molecules whose symmetry is neither spherical nor cylindrical.

Zhang and Forrest[13,14] followed yet another approach in their work on modelling quasiepitaxial ordering at interfaces in organic molecular thin films. Starting with atomistic potentials for PTCDA ($C_{24}O_6H_8$) and NTCDA ($C_{14}O_6H_8$) their goal was to determine the

4

THIS
PAGE
IS
MISSING
IN
ORIGINAL
DOCUMENT

5

degrees of freedom. Atoms can form bonds that hold a molecule together and if we approximate the molecules as rigid, without internal degrees of freedom, we need not calculate these *intra*molecular interactions. Assuming that there are no chemical bonds between different molecules, the *inter*molecular interaction consists of strong short ranged repulsive interactions when molecular cores overlap, and at longer distances the more slowly varying van der Waals and electrostatic interactions. The repulsive and van der Waals interactions are described conveniently together using a Lennard-Jones potential

$$u_{ij}(r_{ij}) = 4\epsilon_{ij} \left[\left(\frac{\sigma_{ij}}{r_{ij}} \right)^{12} - \left(\frac{\sigma_{ij}}{r_{ij}} \right)^{6} \right].$$

(2.1)

where subscripts i and j denote the species of the atoms involved in the interaction and r_{ij} the distance between the two atoms. The electrostatic interactions are caused by the partial charges of the atoms.

A. Pohorille[8] has developed an atomistic potential model for CuPc based on the empirical energy functions and parameters used in CHARMM. Henceforth, we call this the CHARMM model. The relative positions of the atoms inside a molecule are determined by X-ray diffraction studies[16]. Pohorille adjusted partial charges within the molecule to give a potential which agrees well with the β-CuPc crystal structure. To calculate the intermolecular interaction while neglecting the relaxations of the molecules, we need to sum over all the pairs formed by atoms from different molecules; there are $57 \times 57 = 3249$ separate interactions between two CuPc molecules. As mentioned above, it is important to have a more computationally efficient model in any crystal growth study. The approach we have chosen is to replace the atomistic interaction by a smaller number of "site-site" interactions. For the purpose of this exercise we will assume the CHARMM model is exact, and try to adjust the positions of the sites and the interactions between them so that the intermolecular "site-site" potential agrees with the CHARMM model potential for as many relevant configurations as possible.

For two rigid molecules, the configurations form a 6-dimensional continuous space. In principle we could choose a finite number of configurations, represent the positions and

6

interactions of the sites by a set of parameters, and use a multivariable minimization code, e.g. the simulated annealing method[17], to find the values of the parameters which give the best fit. However, the selection of an "objective function", whose minimization corresponds to the best fit of the parameters, is a complicated problem. We cannot fit the details of the short ranged repulsion exactly in any case and the difference between the CHARMM model potential and the "reduced" model potential will certainly be big for those high energy configurations that probe this highly repulsive portion of the interaction. But that does not necessarily mean a bad fit in many practical situations since those high energy configurations contribute little to the partition function or to configurations encountered in crystal growth. It is more important to fit those configurations which have significant attraction correctly while reproducing the overall "size" and "shape" of the molecule. We do not know any systematic way of constructing a physically relevant "objective function" for so complex a system. Therefore our approach is to first understand physically the gross features of interactions of the CHARMM model. Then we try to make our "reduced" model reflect those features we believe to be most important by choosing parameters of the site-site model: the positions and interactions between the sites.

The gross features of the CHARMM model for CuPc can be separated into two parts: 1) the geometric "shape" of the molecule which is mainly determined by the repulsive forces, and 2) the attraction between molecules. These are closely related to the property of Lennard-Jones potential. At short distances, the potential is harshly repulsive and resembles the hard sphere interaction. The electrostatic and van der Waals interactions on the other hand are smoother at a respectable distance so that the "size" and the "shape" of the molecule is more or less determined by the repulsive part of the Lennard-Jones potential. $D_{ij} = 2^{1/6}\sigma_{ij}$ marks the distance where the Lennard-Jones potential (Eq. (2.1)) reaches its minimum and the force changes from attractive to repulsive. In choosing the parameters for the Lennard-Jones potentials, the CHARMM model uses the combining rules which can be formulated as

$$D_{ij} = (D_{ii} + D_{jj})/2, \tag{2.2}$$

$$\epsilon_{ij} = (\epsilon_{ii}\epsilon_{jj})^{1/2}. \tag{2.3}$$

Therefore in the CHARMM model we need to know only the interaction parameters between atoms of the same species. Eq. (2.2) is analogous to the additive rules for the diameters of physical hard spheres.

The CuPc molecule consists of 57 atoms which are virtually coplanar (Fig. 1); there are seven chemically distinct species of atoms. (A single species of atoms—e.g. nitrogen and carbon—can have different properties depending on their positions in the molecule.) The D_{ii}'s for all species are around 3.7 Å except for the copper and hydrogen atoms which are about 3.0 Å. Effectively, we can think of the short ranged repulsive part of the CHARMM potential as made of 57 partially overlapping hard spheres of almost the same size packed together and taking the "shape" of a square tile approximately. The tile has a side length about 10 Å and a thickness about 3.5 Å. Of course the molecule will be a little bumpy and Fig. 2 illustrate this feature by representing each atom by a sphere with diameter D_{ii}.

The long ranged part of the Lennard-Jones potential and electrostatic interactions mainly contributes to the attraction between molecules. Since the CuPc is electrically neutral and has spatial inversion symmetry about the copper atom, the leading terms in the multipole expansion of the local charge distribution are quadrupoles. Therefore asymptotically the interaction between two rigid and static molecules decreases as fast as $1/r^5$ at large distances. The attraction is much bigger when two molecules come face to face than edge to edge.

To model these features, we use an assembly of "interaction sites" and let each of them take the role of a cluster of atoms in the real molecule. Thus the atomistic potential is reduced to a much smaller number of "site-site" interactions, which we take to be Lennard-Jones potentials. In principle we are free to choose an arbitrary function for "site-site" interaction but there is little to be gained by using a more complicated function. Due to the lack of net electrical charge and dipole moments of an individual molecule, the Lennard-Jones potential is physically reasonable and has an appropriate long ranged behavior. Interactions

involving more than two-body terms would increase the number of calculations tremendously. Also by using spherically symmetric interactions rather than angular directional ones at each site, we can avoid complications in implementation of the reduced potential in a modelling application, e.g. molecular dynamics study, by treating each site as a particle. The calculation of force and torque will then be straightforward.

Having decided on the interaction sites approach and the form of site interactions, the next step is to choose the number and positions of the sites and the parameters for the "site-site" potentials. As in the CHARMM model, we tried to separate the fitting into two parts: first to fit the "size" and "shape" of the molecule, then to fit the attraction between two molecules. This separation is important in guiding our search of the parameters because otherwise we would have to go through a multivariable search which is an immense amount of work.

The minimum number of the interaction sites is easily determined. The arrangement of the interaction sites needs to satisfy a 4-fold rotational symmetry. The D_{ab}'s (we use $a, b \cdots$ to denote the species of "interaction sites" with $a = A, B, C \cdots$ and D_{ab}'s are defined in the same way as those for atomistic interactions) are essentially fixed by the thickness of the real molecule, which is about 3.5 Å. Therefore in order to get a side length of about 10 Å without leaving big "holes" in the middle we need at least nine "interaction sites". The arrangement of the sites (see Fig. 3(a)) assumes a 4-fold rotational symmetry and reflection symmetry and there are three distinct species of sites. The distance of each site from the center is so chosen to give the right size of the molecule. Thus in order to provide an adequate description of the "size" and the "shape" of the molecule, most of the repulsive force parameters are fixed to a certain range and we have relatively little freedom to adjust them.

Next we fit the remaining parameters, which are essentially the ϵ_{ab}'s of the "site-site" interaction, to the attractive part of the CHARMM model. Unlike Eq. (2.2), Eq. (2.3) is not very well substantiated physically, and we gain flexibility by using more general combining rules for ϵ_{ab}'s of the "interaction sites".

There are several features of the CHARMM potential which deserve special attention

when attempting a reduction of the potential. In Fig. 4(a) we show the CHARMM potential between two parallel molecules with equal orientation and fixed vertical displacement of 3.4 Å, plotted as a function of horizontal displacement along two coordinates. It seems plausible that such "sliding" configurations, which maximize attractive overlap, will be very important in the crystal growth process as well as in the statistics of equilibrium crystal structures. Therefore it is very important to fit these configurations as accurately as possible. For two parallel molecules sliding past each other at a fixed and not too small distance, the interaction between them is smooth in all directions. This feature underscores the similarity between the molecule and a square tile. The potential reaches its minimum when the centers of the two molecules are slightly displaced. This probably plays a role in the frequently observed CuPc herring-bone crystal structure. Since for each molecule the CHARMM potential has 57 interaction sites, the area where two parallel molecules have significant attractions is very wide. In effect the attraction is spread out over all 57 atoms in the molecule. For our reduced potential model, due to the small number of interaction sites, it is very hard to distribute the attraction widely enough, and we could only satisfy this smoothness feature qualitatively. Although it is possible to fit any one of these configurations much more closely, inevitably this will reduce the quality of other configurations. Our aim is to have a relatively robust qualitative model that will work for as many situations as possible. In those studies that don't involve general configurations, one could adjust the parameters to fit those particular configurations of interest better. To some degree our model is a compromise that includes as much physics as possible without using too many sites.

After extensive study of this "9-site-model", we felt that there were still significant discrepancies with the CHARMM model, which were especially severe for the configurations when site-A of one molecule falls into the gap between the type-B sites of the other one. We are obliged to put four additional sites (see Fig. 3(b)) to fill the gap and since that is their only role, they do not need to interact with every species of site; we choose them to interact with type-A sites only. That will increase the number of separate pairs from 81 for the "9-site-model" to 89. The "13-site-model" gives a potential which is relatively

smooth when the molecules slide past each other in all directions. Fig. 4(b) is the two dimensional energy surface for the reduced model potential with 13 interaction sites. From the spacing of the contours one can see that the potential minimum is much wider for the CHARMM potential and we are not able to achieve complete quantitative agreement with it. There are simply not enough sites in our model to spread out the attractions enough. Fig. 5 shows the comparison of the CHARMM and reduced potentials for two representative sliding directions. Our model potential breaks down much more severely when the molecules are very close to each other and the repulsion is high as illustrated in Fig. 6. However, since these configurations are not expected to appear often and contribute little to the statistics of the crystal structure, we think the reduced potential is adequate for many studies. The parameters are listed in Table I. The distance between type-A and type-B sites is 7.0 Å, and the distance between type-A and type-C sites is 4.7 Å.

There are three distinct stages in our development of a reduced potential fit to the CHARMM model. First, by choosing the right diameters and positions of the sites, we can get a good description of the "size" and "shape" of the molecule. Then by using appropriate "site-site" interactions, we obtain the right long ranged behavior. Finally, by fine-tuning the remaining parameters, we achieve as good a quantitative agreement with the "exact" potential as we can.

III. CRYSTAL STRUCTURES

Though we have fit the gross features of the reduced potential to the full atomistic potential, many differences between the two functions remain. Here we discuss the resulting differences in bulk crystal structure, as determined via energy minimization.

To determine stable (and metastable) zero temperature crystal structures for a given potential, we located minima in a total energy function of many variables which parametrize the structure of the unit cell. We carried out such a calculation for the case of two (rigid) molecules per unit cell, for both the CHARMM potential and the reduced potential. The

total number of variables parameterizing the crystal structure is 18: nine corresponding to the components of three vectors defining the unit cell; three corresponding to the vector locating the second particle in the unit cell; and six corresponding to the orientation angles of the two molecules. Symmetry allows this number to be reduced. However in hopes of avoiding barriers to finding local minima, we chose to minimize over all 18 variables. This choice did not prevent the minimization code[18] from converging, though it likely increased the computation time unnecessarily.

For the CHARMM potential, we found two local minimum energy structures with comparable energies. The first, shown in Fig. 7(a,b), is extremely close to the known herringbone β-CuPc structure (pictured in Ref.[2]); this was not unexpected, as Pohorille fit the partial charges in the CHARMM model specifically to give a low energy for the β-CuPc structure. This herringbone structure has energy= -120.84 kcal/mole. We also found a "flat" structure, shown in Fig. 7(c). Here the two molecules in the unit cell are approximately degenerate, so there is actually only one molecule/unit cell. The flat structure has energy=-118.2 kcal/mole.

For the reduced potential, we also found two structures. First, we found a herringbone structure, shown in Fig. 8(a,b), which resembles—but is not identical to—the α-CuPc structure (pictured in Ref.[2]). This herringbone structure has energy=-116.1 kcal/mole. We also found a "flat" structure in which the two molecules in the unit cell are approximately degenerate, shown in Fig. 8(c). This flat structure has energy=-121.2 kcal/mole. The volume per unit cell is somewhat smaller for this structure than for the CHARMM flat structure discussed above.

In working with the reduced potential, we did not find a local minimum close to the β-CuPc structure. However the search over parameter space required in the minimization over multiple variables is difficult. Though we started the minimization from several different initial conditions—including the β-CuPc structure itself—we cannot be sure that a stable β-CuPc-related crystal phase does not exist for the reduced potential. Likewise, in our work with the CHARMM potential, we did not find an α-CuPc related crystal, but that may be

12

because our search was not thorough enough.

However, a closer look at the exact form of the two potentials yields further insight into the observed crystal structures. In the α-CuPc structure, molecules within a column are stacked so that the center of each molecule is only slightly offset from the one below; while in the β-CuPc structure the offset is larger. We turn again to the potential curves for one molecule sliding over another, plotted in Fig. 5. From these curves we see that the reduced potential favors a small offset; that is, energy is minimized when parallel molecules are shifted only slightly, as in the α-CuPc structure. In contrast, the CHARMM potential favors a larger offset, as in the β-CuPc structure. While this one aspect of local packing is not the only factor affecting the choice of crystal structure, it is perhaps the most important, and appears to explain why the two potentials favor different structures.

Roughly speaking, crystal structure is determined by the need to optimize attractive interactions while ensuring that the repulsive "hard" cores do not overlap. In the case of CuPc, these considerations favor stacked columnar configurations where molecules are packed as closely together as the size of the repulsive cores will allow, while maximizing attractive interactions from adjacent molecular faces. Since CuPc prefers some amount of offset between molecules in a column, straight columns are somewhat less energetically favorable; columns can be uniformly tilted, as in the flat phases shown in Figs. 6(c) and 7(c); or the tilts can alternate, as in the herringbone phases shown in Figs. 6(a,b) and 7(a,b). It is important to note that these different types of structures are nearly degenerate in energy, varying by only a few percent, regardless of which potential is studied. That is, as long as local packing is more or less optimized, the rest of the details of the crystal structure do not change the total energy very much. This finding helps to understand the experimental observation that the crystal structure of a CuPc thin film grown from the vapor phase depends sensitively on the structure of the underlying substrate[19].

We conclude from this analysis that both the CHARMM and reduced potentials show at least some agreement with experimentally observed crystal structures. Both potentials display herringbone structures characteristic of Phthalocyanines, as well as "flat" phases.

Because x-ray studies of polymorphs of CuPc other than α- and β-CuPc have not been performed, it is not known if the "flat" structure corresponds to another known polymorph[20].

We doubt that any site-site potential, including atomistic potentials such as the CHARMM potential, will be able to reproduce consistently the small energy differences that stabilize different crystal polymorphs. We conclude that the reduced potential appears to be at least roughly consistent with the type of crystal structure common for CuPc; for this reason we are optimistic that it may be used in modelling applications to get at least approximate information about the energetics of microscopic processes, e.g. surface diffusion.

IV. CONCLUSION

Computer modeling of organic molecular thin films is significantly limited by both computer processing time and storage constraints when atomistic potentials are used. In spite of these difficulties, small systems have been modeled using full atomistic potentials. C. D. England et al[21] studied a model of coronene adsorbed on MoS_2. They note that due to limitations of both disk space and processor capability, their computations were limited to a layer of seven coronene molecules over a substrate of size 24 × 24 S-Mo-S units. In related work[22] the same authors modelled a layer composed of 9 Pc molecules over a semiconductor substrate. The authors point out that the small overlayer sizes used make it difficult to draw any hard conclusions about the orientation angle and energies determined from these models. Thus the limitations imposed by the use of an atomistic potential are quite serious; the use of a reduced potential would dramatically reduce both storage and processing requirements and make it possible to model much larger system sizes.

Using the method described in Section II, a computationally efficient potential can be determined for any organic molecular material whose intramolecular degrees of freedom can be neglected. Once this task is complete, theory and modelling may be used to address a host of research questions concerning the growth and structure of organic molecular thin films,

going beyond calculations of interface orientations and energetics. As a first step, crystal structures can be determined through the procedure described in Section III and matched with known polymorphs. Then, the potential may be used to calculate various properties of the bulk crystal, such as elastic constants, interlayer shear strength, and energies/structures of defects. It may also be used to calculate static properties related to the crystal surface, such as anisotropic surface energy, and energies of defects such as steps or dislocations. This type of calculation is especially important for organic molecular materials because surface defects play a critical role in the response and selectivity of thin film sensors[23].

One would also like to implement computationally efficient potentials to investigate the microscopic mechanisms that control crystal growth. A logical choice is to calculate the energy barriers associated with diffusion on any given crystal face. This is a very complicated calculation because orientational degrees of freedom as well as center-of-mass motion play an important role in diffusion, such that a molecule's effective diffusion barrier depends sensitively on its angular orientation. We have already begun such calculations for CuPc and find that this effect is very strong; this work will be described in a subsequent publication[24].

Use of computationally efficient potentials will also make molecular dynamics simulation feasible. However, straightforward simulations of this type are unlikely to provide much insight into the crystal growth process because diffusion barriers are relatively high, so that long time scales inaccessible via molecular dynamics would be required to observe significant growth. Instead, data from a careful study of diffusion mechanisms and barriers can be used as input parameters in a Monte Carlo simulation in which molecules diffuse from one lattice site to another according to stochastic rules, in analogy to work done to model kinetic formation of island shapes on metal surfaces[25]. This type of investigation is particularly needed in light of the recent experimental result of M. K. Debe and R. J. Poirier[26] showing that uniform 1000 Å thick films of an organic red pigment will undergo a transition to a dense random array of crystalline whiskers under annealing in vacuo. The authors assert that in this experiment the formation of whiskers is driven only by surface diffusion, and not by kinetic effects associated with growth, i.e. shadowing.

15

With the development of simplified potentials plus anticipated gains in computer processing speed, we may soon be able to simulate realistic models of these and other such complicated processes in organic molecular thin films. It appears likely that work in this area will lead to new understanding of the fundamental properties of these materials.

ACKNOWLEDGMENTS

REFERENCES

[1] See, for example, A. K. Hassan and R. D. Gould, Phys. Stat. Sol. **A132**, 91 (1992); M. K. Debe, J. Vac. Sci. Technol. **A 10**, 2816 (1991).

[2] S. Dogo, J.-P. Germain, C. Maleysson, and A. Pauly, Thin Solid Films **219**, 244 (1992).

[3] T. Kume. S. Hayashi, and K. Yamamoto, Jap. J. Appl. Phys. I, **32** 3486, (1993); K. Yamamoto, S. Egusa, M. Sugiuchi, and A. Miura, Solid State Commun. **85**, 5 (1993).

[4] S. Dogo, J.-P. Germain, C. Maleysson, and A. Pauli, Thin Solid Films **219**, 251 (1992); Y. Sadaoka, T. A. Jones, G. S. Revell, and W. Gopel, J. Mat. Sci. **25**, 5257 (1990).

[5] M. K. Debe, R. J. Poirier, E. L. Cook, L. R. Miller, M. S. Spiering, and S. P. Floeder, J. Vac. Sci. Technol. **A 8**, 49 (1990); M. K. Debe, R. J. Poirier, D. D. Erickson, T. N. Tommet, D. R. Field, and K. M. White, Thin Solid Films **186**, 257 (1990); M. K. Debe and K. K. Kam, Thin Solid Films **186**, 289 (1990); M. K. Debe and R. J. Poirier, Thin Solid Films **186**, 327 (1990).

[6] K. K. Kam, M. K. Debe, R. J. Poirier, and A. R. Drube, J. Vac. Sci. Technol. **A 5**, 1914 (1987); M. K. Debe, K. K. Kam, J. C. Liu, and R. J. Poirier, J. Vac. Sci. Technol. **A 6**, 1907 (1988).

[7] See, e.g. L. S. Perkins and A. E. DePristo, Surface Sci. **294**, 67 (1993).

[8] A. Pohorille, private communication.

[9] B. R. Brooks, R. E. Bruccoleri, B. D. Olafson, D. J. States, S. Swaminathan, and M. Karplus, J. Comput. Chem. **4**, 187 (1983)

[10] J. Corner, Proc. R. Soc. Lond. **A192**, 275 (1948).

[11] J. G. Gay and B. J. Berne, J. Chem. Phys. **74**, 3316 (1981).

[12] B. J. Berne and P. Pechukas, J. Chem. Phys **56**, 4213 (1972).

[13] Y. Zhang and S. R. Forrest, Phys. Rev. Lett. **71**, 2765 (1993).

[14] S. R. Forrest and Y. Zhang, Phys. Rev. **B 49**, 11297 (1994).

[15] S. R. Forrest, private communication.

[16] C. J. Brown, J. Chem. Soc. A (1968) 2488

[17] W. H, Press, S. A. Teukolsky, W. T. Vetterling, and B. P. Flannery: *Numerical Recipes in FORTRAN: the Art of Scientific Computing–2nd ed.* (Cambridge University Press, Cambridge, 1992)

[18] We used the POWELL subroutine given by W. H. Press et al, ibid, p. 299.

[19] M. K. Debe, R. J. Poirier, and K. K. Kam, Thin Solid Films **197**, 335 (1991).

[20] M. K. Debe, private communication.

[21] C. D. England, G. E. Collins, T. J. Schuerlein, and N. R. Armstrong, in "Chemically Sensitive Interface," American Chemical Society, in press.

[22] C.D. England, G. E. Collins, T. J. Schuerlein, and N. R. Armstrong, "Epitaxial Thin Films of Large Organic Molecules: Characterization of Phthalocyanine and Coronene Overlayers on the layered semiconductors, MoS_2 and SnS_2," *Langmuir*, in press.

[23] G. E. Collins, N. R. Armstrong, J. W. Pankow, C. Odeon, R. Brina, C. Arbour, and J.-P. Dodelet, J. Vac. Sci. and Tech. **A 11**, 1383 (1993).

[24] R. L. B. Selinger, D. J. Liu, and J. D. Weeks, "Modelling organic molecular thin films: energetics and mechanisms of surface diffusion," in preparation.

[25] S. Liu, Z. Zhang, G. Comsa, and H. Metiu, Phys. Rev. Lett. **71**, 2967 (1993).

[26] M. K. Debe and R. J. Poirier, J. Vac. Sci. and Tech., in press.

FIGURES

FIG. 1. Chemical constituents of CuPc.

FIG. 2. Picture of the CuPc molecule representing each atom by a sphere.

FIG. 3. Positions of the "interaction sites" for (a) 9-site model and (b) 13-site model.

FIG. 4. The two dimensional dimer energy for (a) CHARMM model and (b) reduced potential model for two parallel molecules with the same orientation.

FIG. 5. Comparison of CHARMM model (solid line) and reduced potential model (dashed line) for two parallel molecules with interplanar distance of 3.4 Å. (a) shows the comparison when the molecules slide along the diagonal direction of Fig. 1 or 3; (b) x-axis.

FIG. 6. Comparison of CHARMM model (solid line) and reduced potential model (dashed line) for two parallel molecules with interplanar distance of 2.8 Å.

FIG. 7. Crystal structures obtained by finding local minima of total intermolecular energy function of a unit cell. For CHARMM potential, two different structures are found: (a) and (b) show the first structure, which is close to the herringbone β-CuPc structure, from two viewing directions; another "flat" structure which is shown in (c) is also found.

FIG. 8. (a) and (b) show the herringbone structure found by energy minimization using the reduced potential. It is close to—but not identical to—the α-CuPc structure. As in the case of CHARMM model, a "flat" structure (c) is also found for the reduced potential, where the two molecules in the unit cell are approximately degenerate.

TABLES

TABLE I. Parameters for the site-site interactions for the reduced potential model.

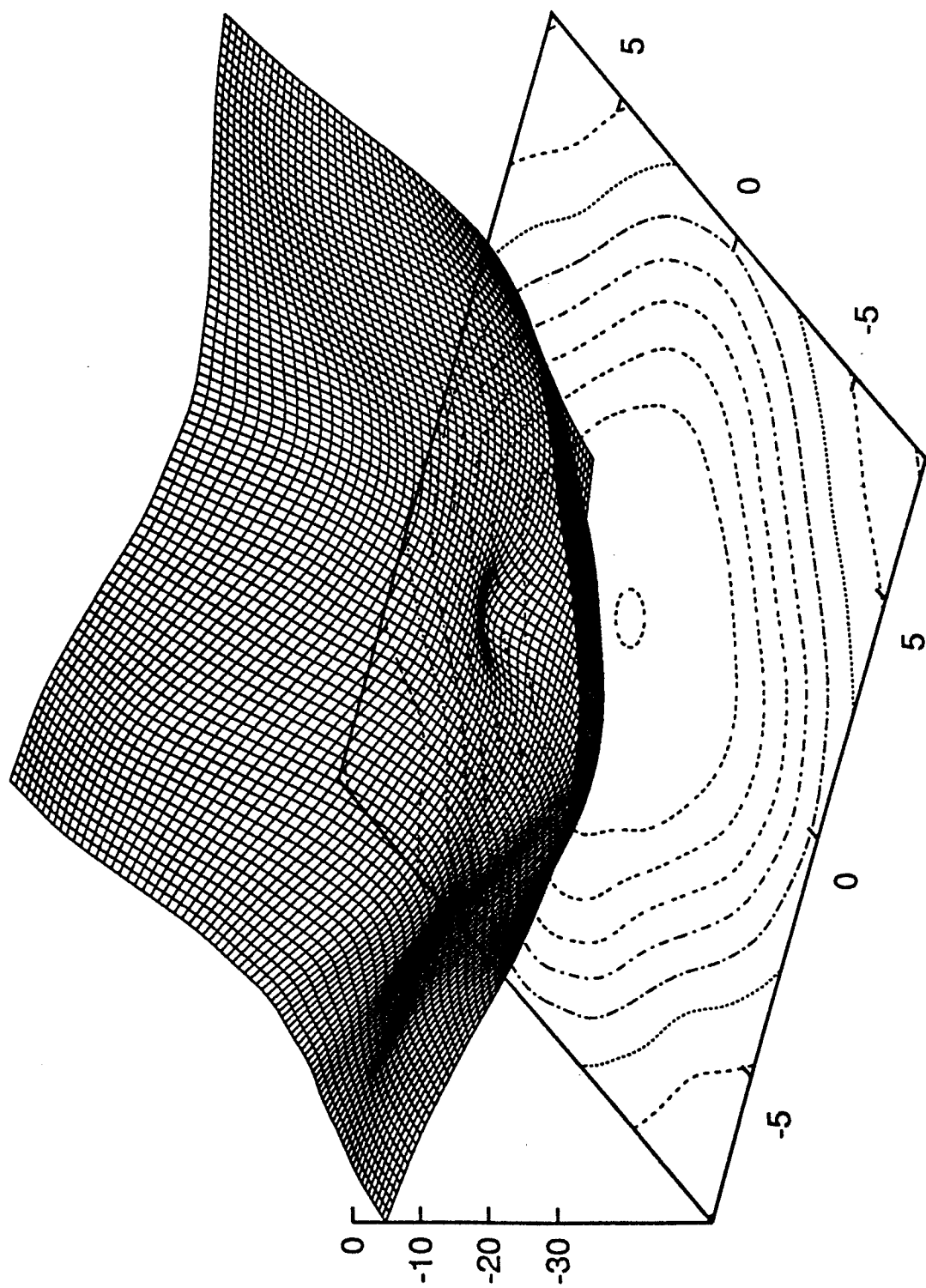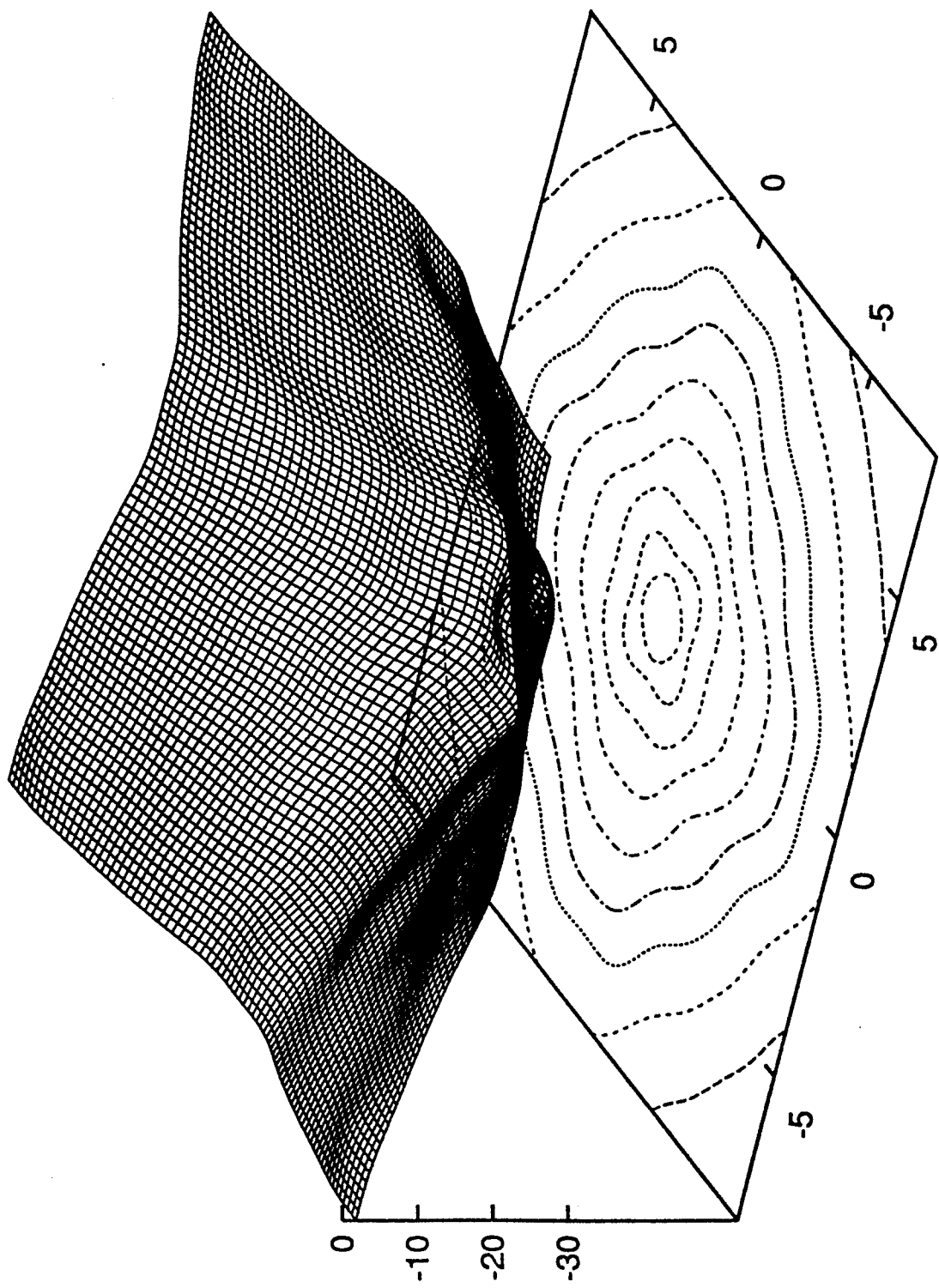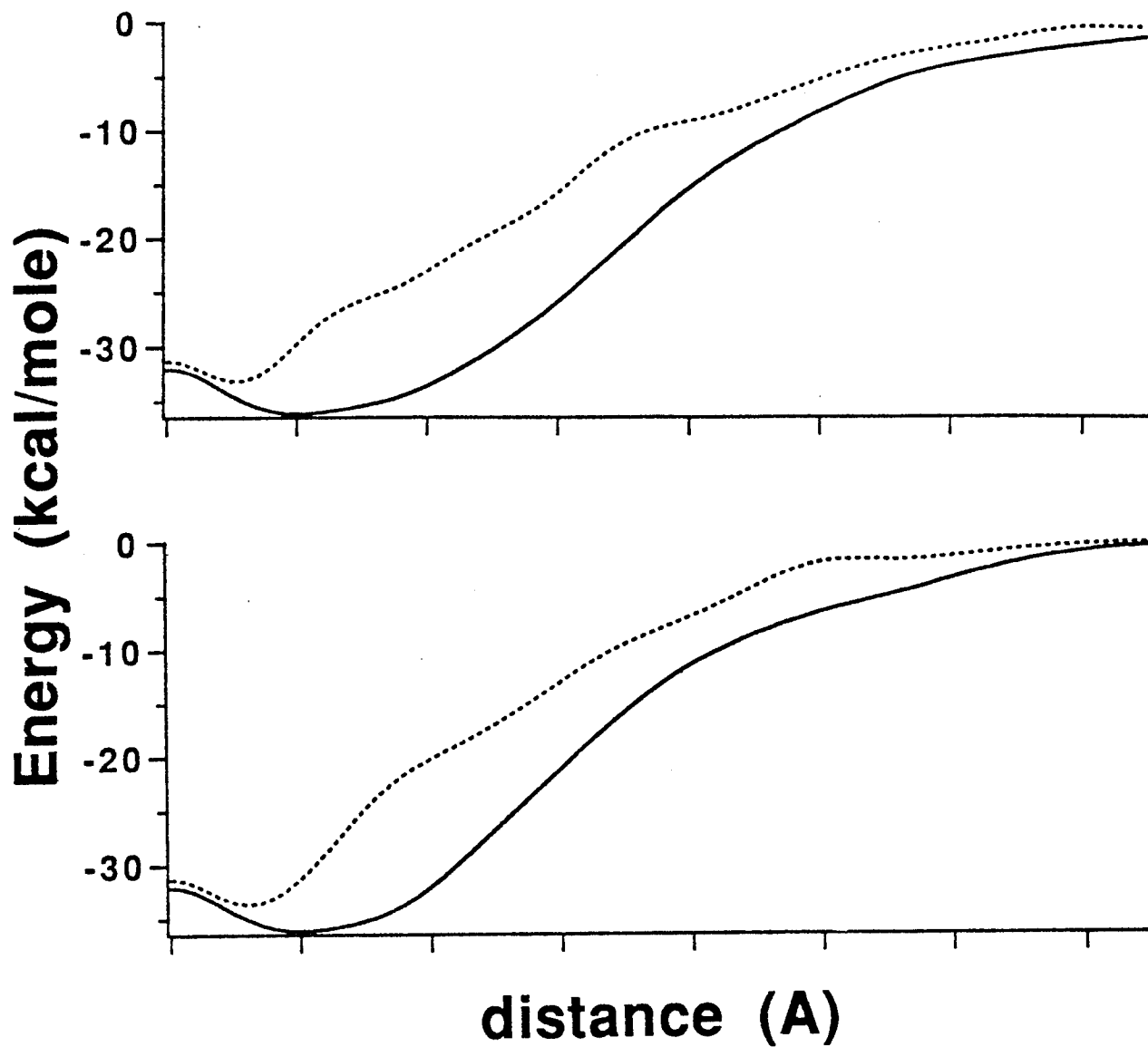| interaction type	$D(\text{Å})$	$\epsilon(\text{kcal/mol})$
$A - A$	4.0	-0.8
$A - B$	3.6	-1.8
$A - C$	3.6	-1.9
$B - B$	3.8	-0.5
$B - C$	3.6	-1.0
$C - C$	3.42	-3.0
$A - D$	3.65	-2.0

Fig. 1

Fig. 2.

Fig. 3.a

Fig.3b

Fig. 4e

Fig. 11b

Fig. 5 (a) & (b)

Fig. 6

Fig. 5a

Figure

Fig. 76

Fig.

Fig.

Fig 20